Mixing A and B Homopolymers with AC Diblock Copolymers: Phase Behavior of Asymmetric Polymer Blends

Natalia A. Denesyuk*,† and Gerhard Gompper‡

Forschungszentrum Jülich, Institut für Festkörperforschung, D-52425 Jülich, Germany

Received February 17, 2006; Revised Manuscript Received May 24, 2006

ABSTRACT: We use grand-canonical-ensemble self-consistent field theory to study blends of both moderately and strongly segregated homopolymers A and B with some diblock copolymer AC, where C is attracted to B. We derive an analytical condition for the Flory−Huggins interaction parameters, which describes a balanced copolymer surfactant AC. We then calculate ternary phase diagrams mainly for blends containing such balanced surfactants. Among the ordered structures, we generally consider lamellar and hexagonal phases, whereas cubic phases are included in the calculation when the polymer blends are studied far from the Lifshitz point. The resulting phase diagrams are highly asymmetric. In particular we show that even a compositionally symmetric polymer blend—that is with equal concentrations and molecular weights of the two homopolymers and with identical polymerization degrees of the copolymer blocks—may organize into either of the two distinct hexagonal structures, as well as into the lamellar structure. One of these hexagonal phases, with the B-rich matrix, has a rather low content of the stabilizing copolymer and may therefore, under experimental conditions, disorder into a polymeric microemulsion. Overall we conclude that the AC diblock can provide a slightly more efficient compatibilizer than its AB counterpart, provided that the incompatibility of homopolymers A and B is not too strong.

1. Introduction

The lack of compatibility between different polymers has been a longstanding problem for the development of new polymeric alloys. In the majority of cases, a binary blend of homopolymers A and B is found in a phase separated state, where the two phases are almost pure liquids A and B.[1] Such phase behavior is due to the large molecular weights of polymers: even if, on the monomer level, the incompatibility between chemical species A and B is fairly weak, it may add up to a very strong repulsion between complete polymer molecules. However many technological applications require mixing of immiscible homopolymers,[2] which can be achieved by adding a "surfactant". Traditionally AB diblock copolymers have been used as such surfactants[3] since their blocks A and B show affinity for the A and B components, respectively, of the homopolymer mixture. This results in the accumulation of copolymer chains at the A/B interface which, in turn, reduces its interfacial tension and drives homopolymers to mix. In this way diblock copolymers are very similar to nonionic surfactants[4] that consist of a hydrophobic tail and a hydrophilic head and that are used to stabilize water/oil microemulsions.[5]

On their own, diblock copolymers form a variety of complex morphological structures[6] such as lamellar, hexagonal, cubic, gyroid, etc., and this phase behavior becomes even more complex upon the addition of homopolymers.[7−10] In fact this tendency of block copolymers to form ordered structures may drive them to segregate in a separate, homopolymer free phase. The latter will inhibit effective mixing of homopolymers A and B since such mixing requires that diblock copolymers spread evenly at the A/B interface. Thus, according to ref 11, to achieve efficient compatibilization the block copolymer must be designed in such a way that its order−disorder transition temperature is lower than the targeted blending temperature. It is either that or the copolymer chains must be sufficiently long for homopolymers to penetrate easily inside the copolymer structures. (We stress that the conclusion of ref 11 was based on polymer blends in which the copolymers were shorter than the homopolymers.) On the other hand high molecular weight copolymers have large reptation times—a disadvantageous factor from the point of view of mixing dynamics.

Notwithstanding these difficulties, the macroscopically homogeneous phase stabilized by a relatively low copolymer content was observed in the A/B/AB mixtures[12−14] and got the name of a polymeric microemulsion. Until very recently this phase could be observed only in blends of slightly immiscible homopolymers A and B. However, in a series of experiments published in refs 15−17, a polymeric microemulsion was stabilized in the A/B/AC blend with highly immiscible homopolymers A and B, where C was attracted to B. The possibility of enhancing the compatibilization efficiency by using AC copolymers (instead of their AB counterparts) had been demostrated in much earlier experimental studies.[18] It was also argued theoretically[19] that in the case of attraction between B and C, homopolymers B can swell the copolymer structure even if they are larger than the structure size. The importance of attractive thermodynamic interactions was also shown experimentally in ref 11, where the PS/PI/PS−PB polymer blend (PS = polystyrene, PI = polyisoprene, PB = polybutadiene) was found in a one-phase state, whereas the PS/PI/PS−PI blend was found in a macrophase separated state. We note that the Flory−Huggins parameter for the PI−PB pair is negative, corresponding to thermodynamic attraction.

The idea of designing balanced surfactants to stabilize polymeric microemulsions was discussed in ref 16. The term "a balanced surfactant" initially refers to nonionic surfactants used in water/oil mixtures, and whose hydrophobic and hydrophilic interactions are comparable in strength.[4] When applied to A/B/AC polymer blends, the condition of balance requires that the A-philic and B-philic tendencies of the AC copolymer are equal. In ref 16, it is also presented as an analytical condition for the Flory−Huggins interaction parameter, $\chi_{BC} \approx 0$. However, fulfilling this condition would essentially take us back to the

* Present address: University of Maryland, Institute for Physical Science and Technology, College Park, MD 20742-2431.
† E-mail: denesyuk@umd.edu.
‡ E-mail: g.gompper@fz-juelich.de.

10.1021/ma060364x CCC: $33.50
Published on Web 07/07/2006

symmetric AB copolymer for which $\chi_{BC} \equiv 0$. We have therefore endeavored to study systematically the phase behavior of A/B/AC polymer blends and to compare it with that of A/B/AB blends. In what follows we assume that C is attracted to B, in agreement with experimental work, although we consider both small and large values of this attraction and introduce our own, analytical criterion for a balanced surfactant. The large number of thermodynamic as well as blend composition parameters results in a very complex phase behavior of ternary polymer blends. In particular, we show that not only the chemical composition of copolymer, but also its relative length with respect to that of homopolymers, have a drastic influence on the copolymer compatibilizing efficiency. Furthermore, we find that the answer to the question whether AB or AC is a better compatibilizer depends strongly on the degree of incompatibility between homopolymers A and B. We use the grand-canonical-ensemble self-consistent field theory (SCFT),[9,10,20,21] which, like any other mean-field theory, does not take into account any fluctuations. This theory is therefore not suitable for the description of a microemulsion phase since bicontinuous microemulsions are known to be stabilized by thermal fluctuations.[22−24] However, in ternary polymer blends the SCFT results have been found to be in good agreement with the experimental measurements of a lamellar phase[17] and of copolymer adsorption at the interface between immiscible homopolymers.[25] In particular, SCFT can be used to determine the minimal copolymer content needed for A/B/AC blends to remain single phase. This in turn can be used as a criterion for judging the copolymer compatibilizing efficiency, as well as for predicting the phase regions where polymeric microemulsions may exist.

The outline of this paper is as follows. In section 2, we give a brief introduction to grand-canonical-ensemble self-consistent field theory and derive SCF equations for A/B/AC mixtures. To look for solutions which correspond to periodic structures, we rewrite these equations in the basis function representation with the basis functions being essentially Fourier harmonics of required symmetry. In section 3.1 we present the derivation of an analytical expression for a balanced surfactant, and in sections 3.2 and 3.3, we compare our numerical results for A/B/AB and balanced A/B/AC blends. The structures that we include in consideration are mainly lamellar and hexagonal, although bcc phases are added in those phase diagrams which correspond to strong segregation (as clearly indicated by the absence of critical points in these diagrams). The grand-canonical-ensemble SCFT can also predict the stability of cocontinuous structures such as the gyroid phase.[26] However we find that the gyroid phase occupies only minor regions in the ternary phase diagrams, and we generally do not consider it in this paper. In section 4, we draw our final conclusions with regard to whether AB or AC is a better compatibilizer, depending on the degree of incompatibility between A and B.

2. Theory

In this section, we generalize the self-consistent field theory developed in refs 9 and 27 for binary A/AB and ternary A/B/AB polymer blends.

We consider a ternary blend of homopolymer chains A and B of polymerization indices $\alpha_A N$ and $\alpha_B N$, respectively, and of copolymer chains AC with an A block of polymerization degree fN and a C block of polymerization degree $(1 - f)N$. In the grand canonical ensemble the number of chains of each type, n_A, n_B, or n_{AC}, is not fixed but regulated by the chemical potentials μ_A, μ_B, and μ_{AC}. We apply the model of an ideal Gaussian chain to describe the flexibility of polymer chains, whereas the binary volume interactions of polymer segments are taken into account by the effective interaction parameters c_{ij}, where i, j = A, B, C. The grand canonical partition function of such a system reads

$$Z = \sum_{n_A=0}^{\infty}\sum_{n_B=0}^{\infty}\sum_{n_{AC}=0}^{\infty}\frac{z_A^{n_A} z_B^{n_B} z_{AC}^{n_{AC}}}{n_A! n_B! n_{AC}!} \times \int\prod_{\nu_A=1}^{n_A} D\boldsymbol{r}_{\nu_A}(s)\exp\left(-\frac{3}{2Nl^2}\int_0^{\alpha_A} ds\left(\frac{d\boldsymbol{r}_{\nu_A}}{ds}\right)^2\right) \times \int\prod_{\nu_B=1}^{n_B} D\boldsymbol{r}_{\nu_B}(s)\exp\left(-\frac{3}{2Nl^2}\int_0^{\alpha_B} ds\left(\frac{d\boldsymbol{r}_{\nu_B}}{ds}\right)^2\right) \times \int\prod_{\nu_{AC}=1}^{n_{AC}} D\boldsymbol{r}_{\nu_{AC}}(s)\exp\left(-\frac{3}{2Nl^2}\int_0^{1} ds\left(\frac{d\boldsymbol{r}_{\nu_{AC}}}{ds}\right)^2\right) \times \exp\left(-\sum_{ij}\frac{c_{ij}}{2}\int\frac{d\boldsymbol{r}}{v}\hat{\Phi}_i(\boldsymbol{r})\hat{\Phi}_j(\boldsymbol{r})\right) \quad (1)$$

where $z_m = \exp(\mu_m/k_BT)$ is the fugacity of polymer chains of type m, v is the reference volume, and l is the statistical segment length which is taken to be the same for all species. The $\hat{\Phi}_i(\boldsymbol{r})$ stands for the dimensionless microscopic density of species i, resulting from a given set of polymer trajectories $\boldsymbol{r}_{\nu_A}(s)$, $\boldsymbol{r}_{\nu_B}(s)$, $\boldsymbol{r}_{\nu_{AC}}(s)$, and the integration in eq 1 is performed over all such sets. The number of interaction parameters in eq 1 can be reduced since the self-consistent field equations include only the linear combinations

$$\chi_{AB} = c_{AB} - \frac{c_{AA}}{2} - \frac{c_{BB}}{2}$$
$$\chi_{BC} = c_{BC} - \frac{c_{BB}}{2} - \frac{c_{CC}}{2}$$
$$\chi_{AC} = c_{AC} - \frac{c_{AA}}{2} - \frac{c_{CC}}{2} \quad (2)$$

the so-called Flory−Huggins parameters, whereas the remaining dependence on c_{AA}, c_{BB}, and c_{CC} appears only in the additive constants to the chemical potentials and effective fields. If, in addition, we require incompressibility of the polymer melt, the fugacity z_{AC} can be eliminated from the self-consistent field equations by introducing the new parameters, $z_1 = z_A(z_{AC})^{-\alpha_A}$ and $z_2 = z_B(z_{AC})^{-\alpha_B}$. Thus, the phase behavior of an incompressible ternary blend can be characterized in terms of only two independent parameters, z_1 and z_2, and eq 1 takes the form

$$Z = \sum_{n_A=0}^{\infty}\sum_{n_B=0}^{\infty}\sum_{n_{AC}=0}^{\infty}\frac{z_1^{n_A} z_2^{n_B}}{n_A! n_B! n_{AC}!} \times \int\prod_{\nu_A=1}^{n_A} D\boldsymbol{r}_{\nu_A}(s)\exp\left(-\frac{3}{2Nl^2}\int_0^{\alpha_A} ds\left(\frac{d\boldsymbol{r}_{\nu_A}}{ds}\right)^2\right) \times \int\prod_{\nu_B=1}^{n_B} D\boldsymbol{r}_{\nu_B}(s)\exp\left(-\frac{3}{2Nl^2}\int_0^{\alpha_B} ds\left(\frac{d\boldsymbol{r}_{\nu_B}}{ds}\right)^2\right) \times \int\prod_{\nu_{AC}=1}^{n_{AC}} D\boldsymbol{r}_{\nu_{AC}}(s)\exp\left(-\frac{3}{2Nl^2}\int_0^{1} ds\left(\frac{d\boldsymbol{r}_{\nu_{AC}}}{ds}\right)^2\right) \times \exp\left(-\sum_{i\neq j}\chi_{ij}\int\frac{d\boldsymbol{r}}{v}\hat{\Phi}_i(\boldsymbol{r})\hat{\Phi}_j(\boldsymbol{r})\right) \quad (3)$$

Following the standard procedure,[10] we insert in eq 3 the identity

$$1 = \int D\Phi_A(\boldsymbol{r})D\Phi_B(\boldsymbol{r})D\Phi_C(\boldsymbol{r})DW_A(\boldsymbol{r})DW_B(\boldsymbol{r})DW_C(\boldsymbol{r}) \times \exp[W_A(\Phi_A - \hat{\Phi}_A) + W_B(\Phi_B - \hat{\Phi}_B) + W_C(\Phi_C - \hat{\Phi}_C)]$$

where the real functions $\Phi_i(\boldsymbol{r})$ and the imaginary functions $W_i(\boldsymbol{r})$ are independent of the specific polymer configurations, unlike the microscopic densities $\hat{\Phi}_i(\boldsymbol{r})$. Performing in eq 3 the summations over n_A, n_B, and n_{AC}, we find

$$Z \propto \int D\Phi_A(\boldsymbol{r})D\Phi_B(\boldsymbol{r})D\Phi_C(\boldsymbol{r})DW_A(\boldsymbol{r})DW_B(\boldsymbol{r})DW_C(\boldsymbol{r}) \times \exp(-\beta F\{\Phi_A,\Phi_B,\Phi_C, W_A, W_B, W_C\}) \quad (4)$$

where $\beta = 1/k_BT$ and F is the free energy functional

$$-Nv\beta F = z_1Q_A + z_2Q_B + Q_{AC} + \int d\boldsymbol{r}[\Phi_A(\boldsymbol{r})W_A(\boldsymbol{r}) + \Phi_B(\boldsymbol{r})W_B(\boldsymbol{r}) + \Phi_C(\boldsymbol{r})W_C(\boldsymbol{r}) - \chi_{AB}N\Phi_A(\boldsymbol{r})\Phi_B(\boldsymbol{r}) - \chi_{BC}N\Phi_B(\boldsymbol{r})\Phi_C(\boldsymbol{r}) - \chi_{AC}N\Phi_A(\boldsymbol{r})\Phi_C(\boldsymbol{r})] \quad (5)$$

In the above equation, Q_m are the partition functions of single polymer chains subjected to the external fields W_A, W_B, and W_C,

$$Q_m = V\left\{\int D\boldsymbol{r}_m(s)\exp\left(-\frac{3}{2Nl^2}\int_0^{\alpha_m}ds\left[\frac{d\boldsymbol{r}_m(s)}{ds}\right]^2\right)\right\}^{-1}\int D\boldsymbol{r}_m(s) \times \exp\left\{-\frac{3}{2Nl^2}\int_0^{\alpha_m}ds\left[\frac{d\boldsymbol{r}_m(s)}{ds}\right]^2 - \int_0^{\alpha_m}dsW_m[\boldsymbol{r}_m(s)]\right\}, \quad m = A, B \quad (6)$$

$$Q_{AC} = V\left\{\int D\boldsymbol{r}_{AC}(s)\exp\left(-\frac{3}{2Nl^2}\int_0^1ds\left[\frac{d\boldsymbol{r}_{AC}(s)}{ds}\right]^2\right)\right\}^{-1}\int D\boldsymbol{r}_{AC}(s) \times \exp\left\{-\frac{3}{2Nl^2}\int_0^1ds\left[\frac{d\boldsymbol{r}_{AC}(s)}{ds}\right]^2 - \int_0^f dsW_A[\boldsymbol{r}_{AC}(s)] - \int_f^1 dsW_C[\boldsymbol{r}_{AC}(s)]\right\} \quad (7)$$

where V is the system volume. A more efficient way of obtaining the partition functions Q_m, as compared to the direct calculation of the path integrals in eqs 6 and 7, is from the end-to-end distance distributions $q_m(\boldsymbol{r}, s)$ of single polymer chains, which are found as the solutions to the following diffusion equations[28]

$$\frac{\partial q_A}{\partial s} = \frac{Nl^2}{6}\Delta q_A - W_Aq_A, \quad 0 < s < \alpha_A \quad (8)$$

$$\frac{\partial q_B}{\partial s} = \frac{Nl^2}{6}\Delta q_B - W_Bq_B, \quad 0 < s < \alpha_B \quad (9)$$

$$\frac{\partial q_{AC}}{\partial s} = \begin{cases}\frac{Nl^2}{6}\Delta q_{AC} - W_Aq_{AC}, & 0 < s < f,\\ \frac{Nl^2}{6}\Delta q_{AC} - W_Cq_{AC}, & f < s < 1\end{cases} \quad (10)$$

where $q_m(\boldsymbol{r}, 0) \equiv 1$ for all types of chains. It is straightforward to check that the Q_m calculated from q_m via

$$Q_A = \int d\boldsymbol{r}q_A(\boldsymbol{r},\alpha_A),\ Q_B = \int d\boldsymbol{r}q_B(\boldsymbol{r},\alpha_B),\ Q_{AC} = \int d\boldsymbol{r}q_{AC}(\boldsymbol{r}, 1) \quad (11)$$

are identical to those calculated from eqs 6 and 7.

The self-consistent field theory amounts to approximating the exact free energy, $F = -T\ln Z$, where Z is given by eq 4, by the value of the free energy functional at its saddle point. Here it is essential to take into account the incompressibility constraint, which can be done by subtracting the term $\int d\boldsymbol{r}\,\zeta(\boldsymbol{r})(\Phi_A + \Phi_B + \Phi_C - 1)$ from eq 5. The saddle point is therefore determined as a solution to the following set of variational equations:

$$\Phi_A = -z_1\frac{\partial Q_A}{\partial W_A} - \frac{\partial Q_{AC}}{\partial W_A} \quad (12)$$

$$\Phi_B = -z_2\frac{\partial Q_B}{\partial W_B} \quad (13)$$

$$\Phi_C = -\frac{\partial Q_{AC}}{\partial W_C} \quad (14)$$

$$W_A = \chi_{AB}N\Phi_B + \chi_{AC}N\Phi_C + \zeta \quad (15)$$

$$W_B = \chi_{AB}N\Phi_A + \chi_{BC}N\Phi_C + \zeta \quad (16)$$

$$W_C = \chi_{AC}N\Phi_A + \chi_{BC}N\Phi_B + \zeta \quad (17)$$

$$\Phi_A + \Phi_B + \Phi_C = 1 \quad (18)$$

We stress that although formally the integration in eq 4 is performed over imaginary fields, the saddle point of the free energy functional, as obtained by solving eqs 12−18, is real. It is therefore only at this stage that we may suggest that W_A, W_B, and W_C play the role of the physical mean fields, produced by all particles (polymer segments) in the system to act upon a particle of a given species.

The first step in solving the variational eqs 12−18 is to calculate the partition functions Q_m. For a periodic ordered phase this can be done most efficiently if we expand all functions of the position vector $\boldsymbol{r}$ in an orthonormal basis set of Laplacian eigenfunctions $f_i(\boldsymbol{r}/D)$, where D is the length of the spatial period.[26] These basis functions are found as a solution to

$$\Delta f_i = -\lambda_i f_i \quad (19)$$

which should possess the symmetry of the phase considered and satisfy

$$\int d\boldsymbol{r}f_i(\boldsymbol{r})f_j(\boldsymbol{r}) = V\delta_{ij} \quad (20)$$

Additionally, we order f_i in such a way that λ_i is a nondecreasing series. In this paper, we will be considering the structures of four different symmetries—lamellar, hexagonal, bcc, and gyroid—which are described by the basis sets given in Appendix A. Equations 8−10 can now be solved exactly for the amplitudes $q^i_A(s)$, $q^i_B(s)$, and $q^i_{AC}(s)$ of the end-to-end distance distributions, defined as

$$q_A(\boldsymbol{r}, s) = \sum_i q^i_A(s)f_i\left(\frac{\boldsymbol{r}}{D}\right) \quad (21)$$

$$q_B(\boldsymbol{r}, s) = \sum_i q^i_B(s)f_i\left(\frac{\boldsymbol{r}}{D}\right) \quad (22)$$

$$q_{AC}(\boldsymbol{r}, s) = \sum_i q^i_{AC}(s)f_i\left(\frac{\boldsymbol{r}}{D}\right) \quad (23)$$

We find

$$q_{\mathrm{A}}^{i}(s) = [\exp(\hat{A}s)]_{i1} \tag{24}$$

$$q_{\mathrm{B}}^{i}(s) = [\exp(\hat{B}s)]_{i1} \tag{25}$$

$$q_{\mathrm{AC}}^{i}(s) = \begin{cases} [\exp(\hat{A}s)]_{i1}, & s < f, \\ \sum_j [\exp(\hat{C}s - \hat{C}f)]_{ij}[\exp(\hat{A}f)]_{j1}, & s > f \end{cases} \tag{26}$$

where the matrices $\hat{A}$, $\hat{B}$, $\hat{C}$ are given by

$$A_{ij} = -\frac{\lambda_i}{d^2}\delta_{ij} - \sum_k \Gamma_{ijk} W_{\mathrm{A}}^{k}$$

$$B_{ij} = -\frac{\lambda_i}{d^2}\delta_{ij} - \sum_k \Gamma_{ijk} W_{\mathrm{B}}^{k}$$

$$C_{ij} = -\frac{\lambda_i}{d^2}\delta_{ij} - \sum_k \Gamma_{ijk} W_{\mathrm{C}}^{k} \tag{27}$$

Here W_{A}^{k}, W_{B}^{k}, and W_{C}^{k} are the amplitudes of the effective fields, defined in full analogy with eqs 21−23, $d^2 = 6D^2/Nl^2$ is the dimensionless period of an ordered structure, and

$$\Gamma_{ijk} = \frac{1}{V}\int \mathrm{d}\boldsymbol{r}\, f_i(\boldsymbol{r}) f_j(\boldsymbol{r}) f_k(\boldsymbol{r}) \tag{28}$$

Now that $q_{\mathrm{A}}^{i}(s)$, $q_{\mathrm{B}}^{i}(s)$, $q_{\mathrm{AC}}^{i}(s)$ are known, the next step is to rewrite the variational eqs 12−18 in such a way that they form a closed set of equations for the amplitudes of the effective fields. We find

$$-z_1\mathscr{D}\frac{\partial q_{\mathrm{A}}{}^{1}(\alpha_{\mathrm{A}})}{\partial W_{\mathrm{A}}^{i}} - \mathscr{D}\frac{\partial q_{\mathrm{AC}}{}^{1}(1)}{\partial W_{\mathrm{A}}^{i}} = K_1(W_{\mathrm{C}}^{i} - W_{\mathrm{A}}^{i}) + K_3(W_{\mathrm{B}}^{i} - W_{\mathrm{A}}^{i}) + K_2\chi_{\mathrm{BC}}N\delta_{\mathrm{i1}} \tag{29}$$

$$-z_2\mathscr{D}\frac{\partial q_{\mathrm{B}}{}^{1}(\alpha_{\mathrm{B}})}{\partial W_{\mathrm{B}}^{i}} = K_2(W_{\mathrm{C}}^{i} - W_{\mathrm{B}}^{i}) + K_3(W_{\mathrm{A}}^{i} - W_{\mathrm{B}}^{i}) + K_1\chi_{\mathrm{AC}}N\delta_{\mathrm{i1}} \tag{30}$$

$$-\mathscr{D}\frac{\partial q_{\mathrm{AC}}{}^{1}(1)}{\partial W_{\mathrm{C}}^{i}} = K_1(W_{\mathrm{A}}^{i} - W_{\mathrm{C}}^{i}) + K_2(W_{\mathrm{B}}^{i} - W_{\mathrm{C}}^{i}) + K_3\chi_{\mathrm{AB}}N\delta_{\mathrm{i1}} \tag{31}$$

where $\mathscr{D} = K_1\chi_{\mathrm{AC}}N + K_2\chi_{\mathrm{BC}}N + K_3\chi_{\mathrm{AB}}N$ and

$$K_1 = \chi_{\mathrm{AC}} - \chi_{\mathrm{AB}} - \chi_{\mathrm{BC}}$$

$$K_2 = \chi_{\mathrm{BC}} - \chi_{\mathrm{AC}} - \chi_{\mathrm{AB}}$$

$$K_3 = \chi_{\mathrm{AB}} - \chi_{\mathrm{BC}} - \chi_{\mathrm{AC}} \tag{32}$$

Usually eqs 29−31 are solved for a set of different length scales d, and in a final step the free energy is minimized with respect to d. However, it provides a much faster algorithm if the free energy is minimized with respect to d at the stage of deriving all other variational equations. This will add just one extra equation

$$z_1\frac{\partial q_{\mathrm{A}}{}^{1}(\alpha_{\mathrm{A}})}{\partial d} + z_2\frac{\partial q_{\mathrm{B}}{}^{1}(\alpha_{\mathrm{B}})}{\partial d} + \frac{\partial q_{\mathrm{AC}}{}^{1}(1)}{\partial d} = 0 \tag{33}$$

to the system of an already very large number of equations. And it is straightforward to see that both approaches should give identical results.

Once eqs 29−31 and 33 are solved with respect to W_{A}^{i}, W_{B}^{i}, W_{C}^{i}, and d, the amplitudes of the polymer segment densities can be calculated from

$$\Phi_{\mathrm{A}}^{i} = -z_1\frac{\partial q_{\mathrm{A}}{}^{1}(\alpha_{\mathrm{A}})}{\partial W_{\mathrm{A}}^{i}} - \frac{\partial q_{\mathrm{AC}}{}^{1}(1)}{\partial W_{\mathrm{A}}^{i}} \tag{34}$$

$$\Phi_{\mathrm{B}}^{i} = -z_2\frac{\partial q_{\mathrm{B}}{}^{1}(\alpha_{\mathrm{B}})}{\partial W_{\mathrm{B}}^{i}} \tag{35}$$

$$\Phi_{\mathrm{C}}^{i} = -\frac{\partial q_{\mathrm{AC}}{}^{1}(1)}{\partial W_{\mathrm{C}}^{i}} \tag{36}$$

and the free energy of a periodic (or liquid) phase is given by

$$-N\upsilon\beta F = z_1 q_{\mathrm{A}}{}^{1}(\alpha_{\mathrm{A}}) + z_2 q_{\mathrm{B}}{}^{1}(\alpha_{\mathrm{B}}) + q_{\mathrm{AC}}{}^{1}(1) + \sum_i [\Phi_{\mathrm{A}}^{i}W_{\mathrm{A}}^{i} + \Phi_{\mathrm{B}}^{i}W_{\mathrm{B}}^{i} + \Phi_{\mathrm{C}}^{i}W_{\mathrm{C}}^{i} - \chi_{\mathrm{AB}}N\Phi_{\mathrm{A}}^{i}\Phi_{\mathrm{B}}^{\mathrm{i}} - \chi_{\mathrm{BC}}N\Phi_{\mathrm{B}}^{i}\Phi_{\mathrm{C}}^{i} - \chi_{\mathrm{AC}}N\Phi_{\mathrm{A}}^{i}\Phi_{\mathrm{C}}^{i}] \tag{37}$$

In general, there can be more than one solution to the variational equations, corresponding to metastable phases. It is therefore important to look for the equilibrium phase, which has the lowest free energy among all other metastable phases, to construct the phase diagram. The SCFT algorithm described above requires that we know the symmetry of potential equilibrium phases a priori. We base our choice of symmetries on the results for the phase behavior of binary A/AB[9] and ternary A/B/AB[27] polymer blends, where the dominant lamellar, hexagonal and bcc phases have been found. Other more complex phases such as gyroid, double-diamond, and hexagonally perforated lamellar structures, have also been examined for the binary A/AB blends.[9] Since, generally, such structures occupy fairly small regions in the phase space, we leave them out in our calculations (the gyroid phase is included in one of the diagrams presented below). Once an equilibrium phase of certain symmetry has been found at least for one set of blend parameters and any blend composition, its field amplitudes can then be used as an initial condition when looking for the same phase for slightly different blend parameters and/or blend compositions, and so on. This way we always track the ordered phases from those of the pure diblock copolymer melt whose phase behavior is well established. Occasionally the algorithm may still converge into a metastable phase which, in most cases, can be detected immediately due to a substantially higher free energy of such phases. It is then necessary to take smaller steps when moving in the blend parameter space.

The Fourier coefficients for each physical quantity form an infinite series which has to be truncated, and this produces some numerical errors. In our calculations, we choose the number of basis functions such that the phase boundaries are determined with less than 1% error. For the highly swollen hexagonal phases this often requires 250 basis functions; we have also made an attempt to calculate a swollen bcc phase with 600 functions, which is the maximum number we can manage computationally.

3. Results and Discussion

3.1. The Formula for a Balanced Surfactant. We are primarily interested in the phase behavior of polymer blends

with χ_{BC} negative. It is quite clear though that if χ_{BC} is negative and large, that is, if the attraction between species B and C is very strong, the copolymer chains will be found mainly in the B-rich phase. We show now that there exists an optimal value of χ_{BC} for which the A-philic and B-philic tendencies of the AC chains balance each other, thus causing these chains to locate at the A/B interface.

For this purpose let us consider only the homogeneous phases. In this case, the Fourier harmonics with $i \geq 2$ are zero for all the physical quantities, and eqs 24−26 reduce to

$$q_A^{\,1}(\alpha_A) = \exp(-\alpha_A W_A^{\,1})$$
$$q_B^{\,1}(\alpha_B) = \exp(-\alpha_B W_B^{\,1})$$
$$q_{AC}^{\,1}(\alpha_{AC}) = \exp[-fW_A^{\,1} - (1-f)W_C^{\,1}] \qquad (38)$$

Substituting these expressions in eqs 34−36 and introducing the homopolymer densities ϕ_{Ah} and ϕ_{Bh}, such that

$$\Phi_A^{\,1} = \phi_{Ah} + f(1 - \phi_{Ah} - \phi_{Bh})$$
$$\Phi_B^{\,1} = \phi_{Bh}$$
$$\Phi_C^{\,1} = (1-f)(1 - \phi_{Ah} - \phi_{Bh}) \qquad (39)$$

we find

$$W_A^{\,1} = -\frac{1}{\alpha_A}\ln\frac{\phi_{Ah}}{z_1\alpha_A}$$
$$W_B^{\,1} = -\frac{1}{\alpha_B}\ln\frac{\phi_{Bh}}{z_2\alpha_B}$$
$$W_C^{\,1} = \frac{1}{1-f}\left[\frac{f}{\alpha_A}\ln\frac{\phi_{Ah}}{z_1\alpha_A} - \ln(1 - \phi_{Ah} - \phi_{Bh})\right] \qquad (40)$$

We can now rewrite the free energy given by eq 37 in terms of ϕ_{Ah} and ϕ_{Bh},

$$N\nu\beta F = \frac{\phi_{Ah}}{\alpha_A}\ln\frac{\phi_{Ah}}{z_1\alpha_A e} + \frac{\phi_{Bh}}{\alpha_B}\ln\frac{\phi_{Bh}}{z_2\alpha_B e} + (1 - \phi_{Ah} - \phi_{Bh})\ln\frac{1 - \phi_{Ah} - \phi_{Bh}}{e} + U \qquad (41)$$

where U is the energy of pair interactions between different species,

$$U = \chi_{AB}N\phi_{Bh}[\phi_{Ah} + f(1 - \phi_{Ah} - \phi_{Bh})] + \chi_{BC}N\phi_{Bh}(1-f)(1 - \phi_{Ah} - \phi_{Bh}) + \chi_{AC}N(1-f)(1 - \phi_{Ah} - \phi_{Bh})[\phi_{Ah} + f(1 - \phi_{Ah} - \phi_{Bh})] \qquad (42)$$

Equations 41 and 42 are equivalent to the Flory−Huggins expression for the free energy in the grand canonical ensemble. If we now assume $f = {}^1/_2$ and

$$\chi_{AC} = \chi_{AB} + \chi_{BC} \qquad (43)$$

then the interaction energy U takes the following quadratic form,

$$U = \frac{\chi_{AB}N}{4}(1 - \eta^2) + \frac{\chi_{BC}N}{4}(1 - \xi^2) \qquad (44)$$

where $\xi = \phi_{Ah} + \phi_{Bh}$ and $\eta = \phi_{Ah} - \phi_{Bh}$. For the same values of $f = {}^1/_2$ and χ_{AC} given by eq 43, the self-consistent eqs 29−31 result in a very simple relationship between ϕ_{Ah} and ϕ_{Bh}

$$(\phi_{Bh} - \phi_{Ah})\chi_{AB}N = \frac{1}{\alpha_B}\ln\frac{\phi_{Bh}}{z_2\alpha_B} - \frac{1}{\alpha_A}\ln\frac{\phi_{Ah}}{z_1\alpha_A} \qquad (45)$$

To obtain analytical results, we additionally assume that $\alpha_A = \alpha_B$. In this case, the coexistence between two homogeneous phases requires $z_1 = z_2$. If $z_1 = z_2$, any solution $\phi_{Ah}^{\,1}$, $\phi_{Bh}^{\,1}$ to eq 45 has a twin solution $\phi_{Ah}^{\,2} = \phi_{Bh}^{\,1}$, $\phi_{Bh}^{\,2} = \phi_{Ah}^{\,1}$. According to eqs 41 and 44, both solutions have the same free energy and correspond, therefore, to the coexisting phases. The resulting equation for the coexistence line,

$$\xi = \eta\coth\left(\frac{h\eta}{2}\right) \qquad (46)$$

where $h = \alpha_A\chi_{AB}N$, depends solely on the homopolymer incompatibility parameter h.

Thus, eq 43 ensures that the coexistence curve of the A-rich and B-rich homogeneous phases of the A/B/AC blend is identical to the (symmetric) coexistence curve of the A/B/AB blend, described by the same values of $\chi_{AB}N$, $\alpha_A = \alpha_B$ and $f = 0.5$.[30] As illustrated in Figure 1, a significant deviation from eq 43 causes the two coexisting liquid phases of the A/B/AC blend to be rather asymmetric with respect to the copolymer concentration. We therefore view eq 43 as the formula for a balanced surfactant—it is different from and less restrictive than the criterion suggested in ref 16, which is $\chi_{BC} \approx 0$. The latter criterion follows from the requirement that the interfaces between A-rich and B-rich domains in a microstructure are flat rather than curved, which is an important factor if one aims at a bicontinuous microemulsion. Correspondingly, our results show that taking $\chi_{BC} < 0$ drives the regions of stability of the hexagonal phase with the B-rich matrix to expand at the cost of the lamellar regions. A possible way to "flatten" the interfaces in such a hexagonal phase would be to increase the length f of the copolymer block A. This possibility is considered in section 3.3 where we present some numerical results for $f \neq 0.5$. The idea of suppressing the interfacial curvature in asymmetric polymer blends by choosing $f \neq 0.5$ has already been discussed in ref 31. Therein an analytical expression for the value of f is given which, in A/B/AB blends with $\alpha_A \neq \alpha_B$, is predicted to correspond to a vanishing spontaneous curvature in the vicinity of the Scott's line[32] of critical blend compositions. We note in passing that the balance criterion (eq 43) has been derived strictly for $f = 0.5$, and in this particular case, it seems to represent the most general definition of a balanced system. However, it would be very interesting to develop this criterion further in order to keep the coexistence curves symmetric also when $f \neq 0.5$.

In any case, it makes sense to consider the question of interface curvature in application to microemulsions only if the formation of interfaces is at all possible at low copolymer content—and this ability is strongly influenced by the balance condition (43). As shown in Figure 1, rather than simply keeping the coexistence curves symmetric, eq 43 also ensures that mixing occurs at the lowest copolymer concentration for all blend compositions and, in particular, for $\phi_{Ah} = \phi_{Bh}$. Thus, violating the balance condition effectively increases the incompatibility degree of the two homopolymers, which will most likely still hold when the microstructures are taken into account. We believe therefore that if eq 43 is fulfilled, the copolymer content required to keep the polymer blend single phase will be minimal. For any given pair of homopolymers, this copolymer content

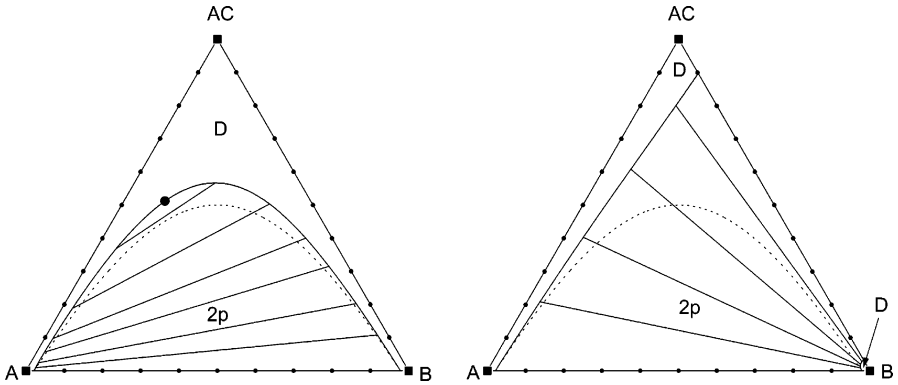

Figure 1. Curves of coexistence of the A-rich and B-rich homogeneous phases in the A/B/AC blends with $\chi_{AC}N_h = 3$, $\chi_{AB}N_h = 4$, $\alpha = 0.5$, $f = 0.5$, and (a) $\chi_{BC}N_h = -4$ or (b) $\chi_{BC}N_h = 2$. As indicated by nonhorizontal tie-lines, significant deviations from eq 43 in either direction lead to coexisting phases which are highly asymmetric with respect to the copolymer content. The same dotted line in both figures shows the entirely symmetric coexistence curve for $\chi_{BC}N_h = -1$ (the corresponding horizontal tie-lines are not shown). The one-phase and two-phase regions are marked by "D" (disordered phase) and "2p", respectively.

can be decreased further by tuning either χ_{BC} or χ_{AC}, whichever of the two we choose as an independent variable. We appreciate of course that in real experiments these parameters are not independent and therefore usually change simultaneously.

We also note that the balance condition (43) does not depend on the polymerization degrees of either copolymers or homopolymers. This is connected to the fact that, similar to eq 46 which is independent of the length ratio α, eq 43 has been derived ignoring any copolymer microstructures. In fact, such microstructures do not form if the copolymer chains are shorter than a certain threshold length, in which case only the overall concentration of copolymer (but not its polymerization degree) determines whether the blend is mixed or macrophase separated. Since the idea of eq 43 is to minimize the copolymer content required to mix A and B when such short copolymer chains are added, this equation is also independent of the copolymer molecular weight. Of course, a more complex balance condition could probably be derived which would also take into account the microstructures formed by long copolymer chains and which would, therefore, depend on the length ratio α. However, an important advantage of eq 43—apart from it being strictly valid for short copolymer chains—is its very simple form.

In this paper we consider polymer blends satisfying eq 43. This means that at low copolymer concentrations—when a macrophase separation into homogeneous A-rich and B-rich phases takes place—the phase diagrams are symmetric with respect to the $\phi_{Ah} = \phi_{Bh}$ isopleth. We note that this does not imply that the ordered phases too are symmetric at higher copolymer concentrations. A similar situation is encountered in water/oil mixtures stabilized by balanced nonionic surfactants, wherein highly asymmetric lamellar phases have been found.[33]

3.2. A/B/AB Blends. The phase behavior of the A/B/AB ternary polymer blends has been studied in great detail by means of both analytical theory[30,34] and self-consistent field calculations.[27,35,36] Here we present just a few diagrams, illustrating the main aspects of this phase behavior, that we find helpful in understanding similar diagrams for the A/B/AC mixtures. There are two types of phase diagrams that we consider in this paper: the first type is the Gibbs triangle, which shows equilibrium phases or multiphase regions for some fixed values of $\chi_{ij}N$, α_A, α_B, f, and all possible blend compositions. We will only look at the systems with $\alpha_A = \alpha_B \equiv \alpha$ and, unless indicated otherwise, with $f = 0.5$. The second type of diagrams are the cuts of the Gibbs triangles along the $\phi_{Ah} = \phi_{Bh}$ isopleth (ϕ_{Ah}, ϕ_{Bh} are the homopolymer concentrations) for the fixed values of $\chi_{ij}\alpha N$, but with varying α. In these diagrams, we show the

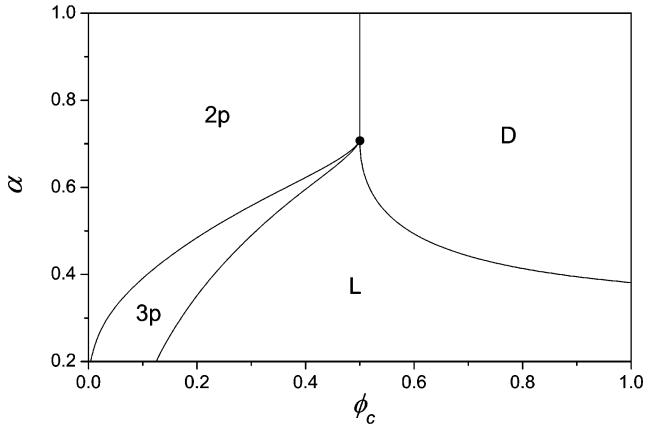

Figure 2. α vs ϕ_c diagram for the compositionally symmetric A/B/AB blends with $\chi_{AB}N_h = 4$. The vertical line represents the Scott's line which ends at the Lifshitz point (full circle). The lamellar phase ("L"), appearing below the Lifshitz point, is bounded by the spinodal line on the right and, on the left, by the line of the first-order transitions into the coexisting A-rich and B-rich homogeneous (or disordered) phases. The one-phase, two-phase and three-phase regions which involve one or more homogeneous phases are marked by "D", "2p", and "3p", respectively.

boundaries of single phase regions in the α vs ϕ_c plane, where ϕ_c is the copolymer concentration. The incentive for constructing such diagrams is to be able to say how much copolymer of what length we should add in the system, to mix a pair of homopolymers with a given degree of incompatibility.

A diagram of the second type is shown in Figure 2 for blends with $\chi_{AB}N_h = 4$, where $N_h = \alpha N$ is the homopolymer degree of polymerization. Such a value of the incompatibility parameter corresponds to a pair of strongly immiscible homopolymers A and B (we recall that the critical point of mixing for the binary homopolymer blend is given by $\chi_{AB}N_h = 2$). The addition of copolymer chains to a phase-separated blend of A and B will drive these homopolymers to mix and form a uniform liquid phase, given that the copolymer concentration is higher than some critical value. This critical concentration of copolymer is given by the Scott's line[32]

$$\phi_c = 1 - \frac{2}{\chi_{AB}N_h} \tag{47}$$

which is independent of the copolymer molecular weight (the vertical line in Figure 2). However, eq 47 does not take into account the formation of ordered structures in the ternary

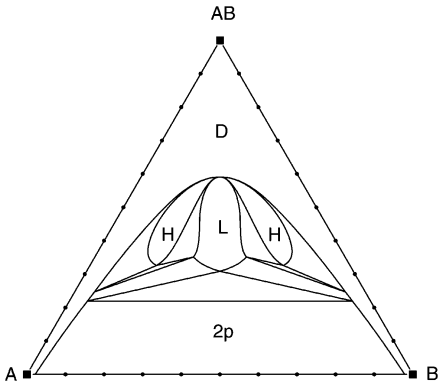

Figure 3. Gibbs triangle for the A/B/AB blend with $\chi_{AB}N_h = 4$ and $\alpha = 0.5$. "L", "H", and "D" indicate the regions of stability of the lamellar, hexagonal, and disordered phases. The triangular regions of three-phase coexistence are separated by the two-phase regions; "2p" marks the largest of the two-phase regions between the A-rich and B-rich homogeneous phases. Note that the pure copolymer is found in the disordered state, whereas the ordered structures appear through a critical point at some smaller ϕ_c.

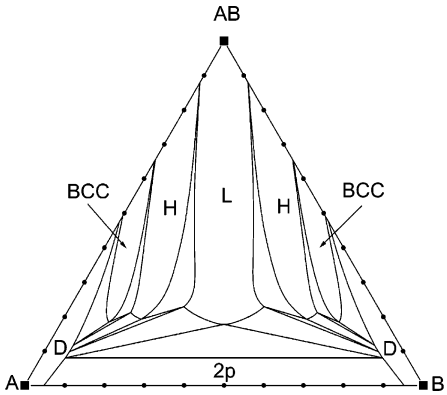

Figure 4. Gibbs triangle for the A/B/AB blend with $\chi_{AB}N_h = 3.3$ and $\alpha = 0.3$. These blend parameters correspond to the region in the α vs ϕ_c diagram (cf. Figure 2) which lies far below the Lifshitz point, hence we have also included the bcc phases. Note that the pure copolymer is found in the lamellar phase and there is no critical point associated with the ordered structures. ("L" is lamellar, "H" is hexagonal, "D" is disordered, and "2p" is liquid−liquid coexistence.)

polymer blends. In fact, if the copolymer chains are long enough, the ternary blend will microphase (rather than macrophase) separate with decreasing the copolymer concentration ϕ_c. For $\phi_{Ah} = \phi_{Bh}$ this microphase separation occurs continuously through the critical point which can be calculated using the random phase approximation (RPA).[37] The derivation of RPA for A/B/AC blends is contained in Appendix B of this paper. For brevity, we will refer to the locus of these critical points, which are shown in Figure 2 for different values of α, as the spinodal line. We note that the order−disorder transition, induced by varying the copolymer concentration ϕ_c, can only be observed in the A/B/AB blends with $\chi_{AB}N < 10.5$. This condition ensures that the pure copolymer is found in the disordered phase,[26] since the energy gain associated with the formation of microdomains, is less significant than the entropy loss due to the chain stretching. The large stretching of chains required in this case is essential to fulfill the incompressibility condition in the areas near the microdomain centers. At the same time, fairly mobile homopolymer chains can easily distribute inside a microdomain structure and lower its free energy by relieving the stress associated with the incompressibility constraint. Hence, for $\chi_{AB}N < 10.5$, "diluting" a copolymer melt with some relatively short homopolymer chains, which on their own cannot form any ordered phases, actually drives this melt to order. In the opposite case of $\chi_{AB}N > 10.5$, the pure symmetric copolymer is found in the lamellar phase, which is also the equilibrium phase for $\phi_c < 1$. In Figure 2 the order−disorder transition of the pure copolymer melt is marked as the crossing point of the spinodal line and the $\phi_c = 1$ axis at $\alpha \approx 0.38$. The crossing point of the spinodal line with the Scott's line is referred to as an isotropic Lifshitz point,[38] and it marks the onset of ordered structures in a given polymer blend. For an A/B/AB polymer blend, the value of α at the Lifshitz point is given by[30]

$$\alpha_L = \frac{\sqrt{\chi_{AB}N_h - 2}}{2} \tag{48}$$

whereas the copolymer concentration is found from eq 47. Thus, in the polymer blend with $\chi_{AB}N_h = 4$, we will only be able to observe some ordered structures if the copolymer chains are longer than $N = \sqrt{2}N_h$ (cf. Figure 2).

The formation of ordered structures is illustrated in Figure 3 which shows a Gibbs triangle for a blend with $\chi_{AB}N_h = 4$ and $\alpha = 0.5$. In this diagram we have included only the lamellar and hexagonal ordered structures, which emerge via a critical point. For small concentrations of copolymer, when its compatibilizing effect is negligible, the polymer blend macrophase separates into an A-rich and a B-rich phase. The triangles in Figure 3 bound the regions of three-phase coexistence, in particular, we see a large, centrally placed region of coexistence between the lamellar and two disordered phases. The coexisting lamellar phase has a quite low copolymer content, approximately 30%, which is remarkable given the strong incompatibility of A and B. Of course, the stability of the lamellar phase with such a low copolymer content is the result of the self-consistent field theory, which does not take into account local concentration fluctuations. We anticipate that, in real polymer blends, this phase may lose its long-range order and transform into a bicontinuous microemulsion. This conclusion is also supported by the fact that in experimental phase digrams,[12,13] the microemulsion phase is always found on the small ϕ_c side of the lamellar phase. Therefore, even if we cannot calculate the properties of a polymeric microemulsion using self-consistent field theory, we can still predict its approximate location in the phase diagram. Since part of our motivation for studying the ternary polymer blends lies in finding the optimal copolymer characteristics for the formation of such microemulsions, we will be paying particular attention to the ordered structures with low copolymer content.

Now let us go back to Figure 2 where we have included the locus of points indicating the lamellar phase, which coexists with the two disordered phases, for $\chi_{AB}N_h = 4$ and different values of α. This line crosses the Scott's and the spinodal lines at the Lifshitz point and identifies the minimal copolymer content at which an ordered structure may still be observed (we note that at $\alpha_A = \alpha_B$, $f = 0.5$, and $\phi_{Ah} = \phi_{Bh}$, only lamellar ordered structures are present). We see that decreasing the value of α, or increasing the size of copolymer chains, extends the region of stability of the lamellar phase to smaller ϕ_c. Thus, from the thermodynamic point of view, the longer copolymer chains are more favorable for the formation of microemulsions.

Figure 4 shows the Gibbs triangle for a polymer blend with $\chi_{AB}N_h = 3.3$ and $\alpha = 0.3$. The incompatibility parameter $\chi_{AB}N = 11$, is larger than its critical value for the order−disorder transition in the pure copolymer melt. Hence the lamellar phase is present at $\phi_c = 1$, and there is no continuous order−disorder transition. In many other aspects this diagram is very similar to

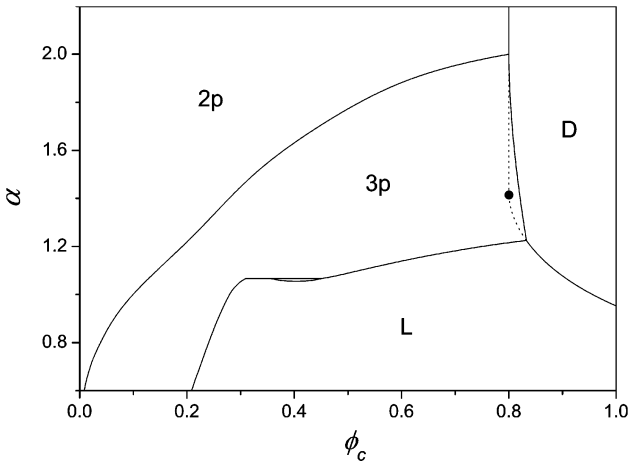

Figure 5. α vs ϕ_c diagram for the compositionally symmetric A/B/AB blends with $\chi_{AB}N_h = 10$. The Lifshitz point (full circle) is found inside the region of three-phase coexistence ("3p") and, therefore, does not correspond to any special physical point. The dotted sections of the Scott's and spinodal lines are included in the same three-phase region. The solid line on the right of the Scott's line indicates one of the three coexisting homogeneous phases ("D"), which has the highest copolymer content and $\phi_{Ah} = \phi_{Bh}$. The very shallow trough in the boundary of the lamellar phase ("L") is the coexistence region of two different lamellar phases, one of which is more swollen than the other. Associated with this first-order transition, is a significant extension of the lamellar phase to low copolymer concentrations.

that shown in Figure 3, except that it also includes the bcc phases. The Gibbs triangle for these values of parameters has already been calculated in ref 27; here, we have recalculated it with a much greater precision, 150 basis functions instead of 50, which has enabled us to get rid of some small artifacts in the bcc phase boundaries.

We have also checked the limits of stability of the lamellar phase for a highly immiscible pair of homopolymers A and B with $\chi_{AB}N_h = 10$. The corresponding α vs ϕ_c diagram is shown in Figure 5. As compared to the diagram in Figure 2, the present Lifshitz point is shifted toward much higher values of $\phi_c = 0.8$ and $\alpha = \sqrt{2}$. There are two other significant differencies from the diagram shown in Figure 2. First, the line which corresponds to the coexistence of the lamellar phase and the two disordered phases, does not go through the Lifshitz point. Instead it crosses the spinodal below the Lifshitz point, where it also meets the line which represents the coexistence of three disordered phases (this line indicates the disordered phase with the highest copolymer content). We note that although in this case the Lifshitz point does not have any physical meaning, it can still be defined formally as a crossing point of the spinodal and the Scott's lines. In contrast to Figure 2, the area just below such a "hidden" Lifshitz point is no longer occupied by the lamellar phase but by the coexistence region of three different disordered phases. This three-phase coexistence region, corresponding to the first-order transition into A-rich and B-rich liquids, is also present above the "hidden" Lifshitz point, where it takes up the place of the continuous transition shown by the Scott's line in Figure 2.

Another significant feature of the diagram in Figure 5 is the existence of the first-order transition between two lamellar phases, one of which is more swollen than the other, i.e., it has a lower copolymer content and rather large value of *d*. (The first-order transition between two symmetric lamellar phases in an A/B/AB blend was first calculated in ref 36. Earlier studies assigned this region in the phase diagram to another first-order transition, between a symmetric and two asymmetic lamellar phases.[35]) Though the coexistence region associated with this transition is extremely shallow, lying between $\alpha = 1.055$ and $\alpha = 1.067$, it is responsible for a prominent intrusion of the lamellar phase in the area of small copolymer concentrations, when $\alpha < 1$. Thus, from a purely thermodynamic point of view, sufficienly long AB diblock copolymers can serve as effective compatibilizers for a pair of strongly segregated homopolymers A and B. However, as we mentioned earlier, very long copolymer chains are expected to have large reptation times which may hinder their even distribution at the A/B interface.

3.3. Balanced A/B/AC Blends. Let us now consider some A/B/AC polymer blends, where species C is attracted to B. Our choice of χ_{ij} is restricted by eq 43 which ensures that, if one takes into account only homogeneous phases, the phase behavior of a ternary blend does not depend on the particular kind of species C. Specifically, the Lifshitz point, as well as the Scott's line to which it belongs, depend only on the value of $\chi_{AB}N_h$. We stress that the latter statements are valid only if $\alpha_A = \alpha_B$ and $f = 0.5$—which is the case for all blends studied here, except for two. The spinodal lines shift to lower copolymer concentrations when the absolute value of $\chi_{BC}N_h$ is increased and $\chi_{AB}N_h$ is kept constant, but only very insignificantly as all these lines have to cross at the same Lifshitz point. Most of the results presented here are for $\chi_{AB}N_h = 4$. The corresponding Gibbs triangles are calculated for moderately segregated blends, hence we take into account only the lamellar and hexagonal ordered structures. We expect that the two bcc phases will occupy fairly small regions in the phase space, situated on the sides of the respective hexagonal phases, but will not change the phase diagrams in any principal way.

Figure 6a shows the Gibbs triangle for the A/B/AC blend characterized by $\alpha = 0.5$ and $\chi_{AB}N_h = 4$, $\chi_{AC}N_h = 3$, and $\chi_{BC}N_h = -1$. This diagram should be compared with its direct A/B/AB analogue, shown in Figure 3. First, the critical point no longer belongs to the $\phi_{Ah} = \phi_{Bh}$ isopleth but is shifted toward higher concentrations of B. We will see that, in general, the ordered structures occupy larger areas on the B-rich side of the Gibbs triangle—this is a result of an easier penetration of homopolymers B inside the copolymer microdomains, due to the attraction between B and C. At the same time, the ordered structures in Figure 6a are observed at copolymer concentrations that are similar to those in Figure 3. This indicates that the system is more sensitive to the changes in χ_{AB} or α rather than in χ_{BC}, given of course that such changes satisfy the balance condition (43). Another interesting feature of Figure 6a is the presence of two hexagonal phases at $\phi_{Ah} = \phi_{Bh}$, one of them with an A-rich matrix and the higher copolymer content than the lamellar phase, and another with a B-rich matrix and rather low ϕ_c. Though it seems obvious that the hexagonal phases should appear for the blend compositions far from the $\phi_{Ah} = \phi_{Bh}$ isopleth, it is quite remarkable to observe these phases for a blend which is symmetric in all other ways except for the negative value of χ_{BC}. To explain the origin of the first of these hexagonal phases, we make the following argument. At high copolymer concentrations ϕ_c, not all of the copolymer chains are localized at the A/B interface but many of them are dissolved inside the A-rich and B-rich domains. At the same time, the average concentration of B in the B-rich cylinders of the hexagonal phase is higher than that in the B-rich lamellae of the lamellar phase. This can be easily understood since the cylinders occupy less than half of the available space but are expected to accommodate 50% of the total homopolymer content. Such high concentration of B inside the cylinders, along with a rather high copolymer concentration, produce a large

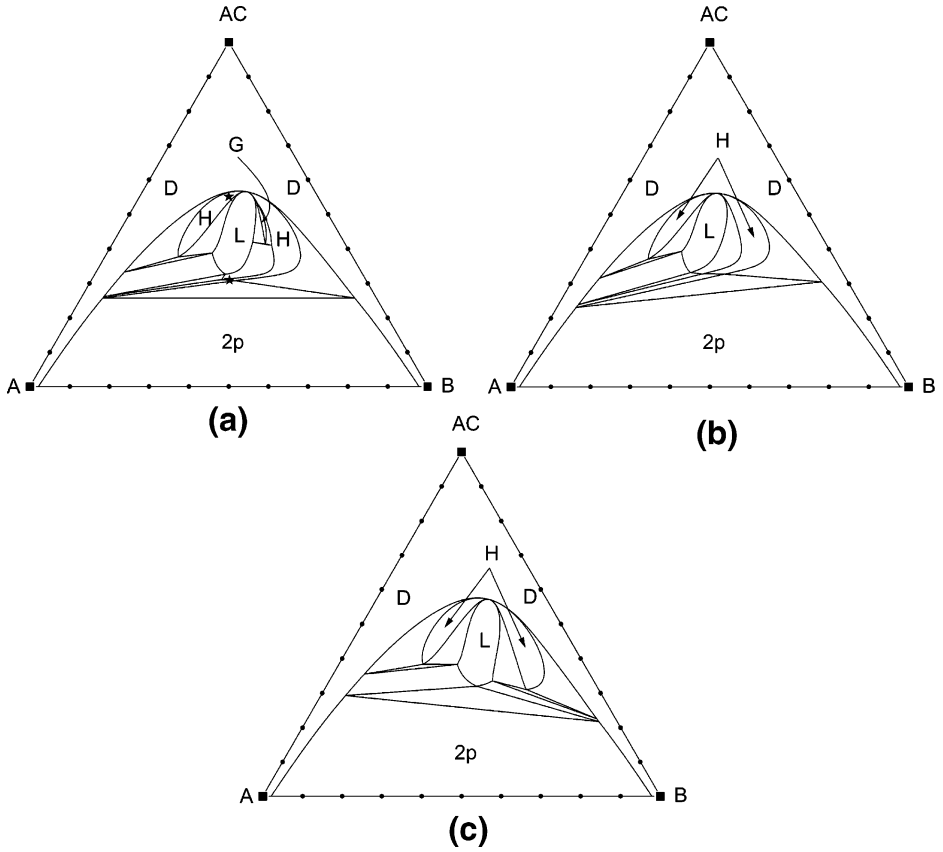

Figure 6. Gibbs triangles for the A/B/AC blends with $\chi_{AB}N_h = 4$, $\chi_{AC}N_h = 3$, $\chi_{BC}N_h = -1$, and $\alpha = 0.5$. Different length ratios of copolymer blocks are considered, namely: (a) $f = 0.5$, (b) $f = 0.48$ and (c) $f = 0.52$. In (a), the small region of stability of the B-rich gyroid phase ("G") is found between the lamellar phase and the hexagonal phase with the B-rich matrix. The two stars in the same figure indicate the blend compositions for the density profiles in Figure 7. ("L" is lamellar, "H" is hexagonal, "D" is disordered, and "2p" is liquid−liquid coexistence.)

number of favorable BC contacts which make the hexagonal phase energetically more stable. Parts a and b of Figure 7 show the density profiles for the stable hexagonal and metastable lamellar phases (in the phase region considered) that support our conclusions. At the same time, when the copolymer concentration ϕ_c is low, the copolymer chains accumulate at the A/B interface, as illustrated in Figure 7, parts c and d. In this case the attraction between B and C draws the B chains toward the interface, so that the number of favorable BC contacts can be increased. The hexagonal phase with the B-rich matrix should therefore be stable, as it allows to accommodate more B near the interface while keeping the total density constant. We note that such a hexagonal phase is characterized by interfaces of very low curvature, which can be seen from the density profiles in Figure 7d. These density profiles (unlike those shown in Figure 7b) are nearly symmetric with respect to an interface, and in fact resemble the lamellar density profiles in Figure 7c. Furthermore, the interfaces between A-rich and B-rich domains in a largely swollen hexagonal phase are barely interacting and can therefore fluctuate easily without disturbing each other. These fluctuations may hide, to a large extent, the low intrinsic curvature of the hexagonal phase.

In Figure 6a the region of stability of the hexagonal phase with the B-rich matrix takes the form of a very narrow channel. It is also a largely swollen phase with the period D having a value of approximately 18 copolymer sizes, as compared to a value of about 6 copolymer sizes near the critical point. We expect that this channel will be rather unstable in the presence of thermal fluctuations which may well transform it into a bicontinuous microemulsion. We have also discovered that it is very sensitive to small deviations of f from the value 0.5. (Such deviations are unavoidable in real, experimental blends since different chemical structures of the two blocks affect f in intricate ways.) This is demonstrated in Figure 6, parts b and c, which shows the Gibbs triangles for the same values of $\chi_{ij}N_h$ and α, but for $f = 0.48$ and $f = 0.52$. We see that for $f \leq 0.48$ the channel of the hexagonal phase becomes more developed, whereas for $f \geq 0.52$ it disappears completely. Remember that the curvature of the cylindrical domains of the B-rich hexagonal phase inside the channel is very low and, as discussed in section 3.1, this curvature may vanish entirely for some $f > 0.5$, which would justify the absence of the hexagonal channel for $f \geq 0.52$. Yet, increasing f corrects only some selected parts of the phase diagram while the rest of it becomes even more asymmetric—in particular, the critical point and the microphase regions are shifted to the B-rich side of the Gibbs triangle. We also note that the ordered structures are observed at slightly lower copolymer concentrations in the blend with $f = 0.5$, than in the two other blends. The reason is that changing the value of f effectively leads to the violation of the condition for a balanced surfactant, given in eq 43 and derived for $f = 0.5$. Thus, although the balance criterion was initially derived for homogeneous phases, it ensures that mixing occurs at the lowest copolymer concentration also when the microphases are taken into account.

Decreasing the value of α, i.e., moving away from the Lifshitz point, leads to a vast expansion of the ordered structures and consequently, to the disappearance of the critical point. This is illustrated in Figure 8 for slightly different values of the interaction parameters than those studied above, that are $\alpha =$

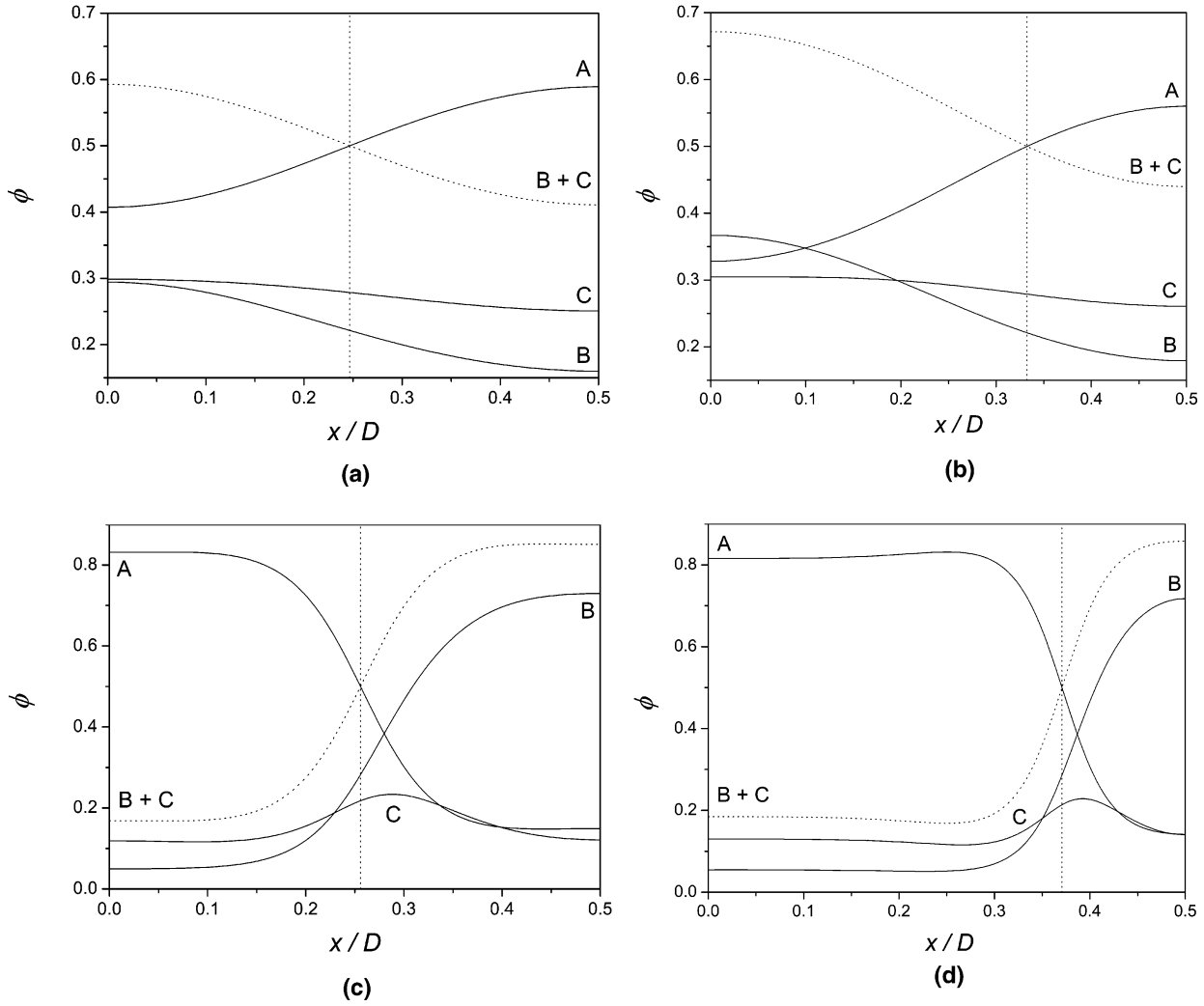

Figure 7. $\Phi_i(x)$ density profiles for the two blends indicated with the stars in Figure 6a. (For the hexagonal phases we take $y = 0$.) Shown are the density profiles (a) in the metastable lamellar phase with the higher copolymer content, (b) in the stable hexagonal phase with the A-rich matrix, (c) in the metastable lamellar phase with the lower copolymer content, and (d) in the stable hexagonal phase with the B-rich matrix. The dotted curves are for $\Phi_B(x) + \Phi_C(x)$, and the vertical dotted lines mark the A/B interface.

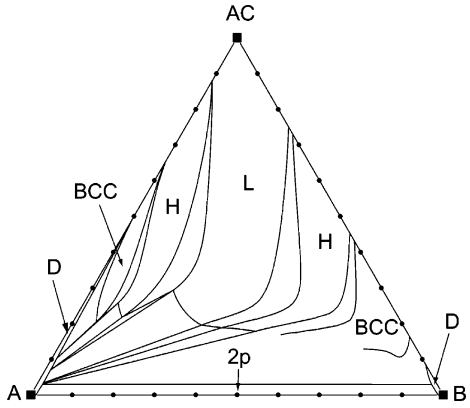

Figure 8. Gibbs triangle for the A/B/AC blend with $\chi_{AB}N_h = 4.5$ and $\chi_{BC}N_h = -1.2$; all other parameters and designations are those in Figure 4. The calculation of the B-rich bcc phase could not be completed due to the computational difficulties. We see that the channel of the B-rich hexagonal phase remains stable also in highly segregated blends.

0.3 and $\chi_{AB}N_h = 4.5$, $\chi_{AC}N_h = 3.3$, and $\chi_{BC}N_h = -1.2$. This diagram is a direct analogue of the symmetric diagram shown in Figure 4. We observe the same main features as in the previous diagrams, except that the hexagonal phase with the A-rich matrix is no longer stable on the $\phi_{Ah} = \phi_{Bh}$ isopleth. However, at low copolymer concentrations, there is still a narrow channel of the hexagonal phase with the B-rich matrix. We see that it reaches as far as the $\phi_{Ah} = \phi_{Bh}$ isopleth, also when the bcc phase is taken into consideration. Unfortunately, we were not able to complete the calculation of the bcc phase in the central part of the Gibbs triangle, as it gets very swollen and more than 600 basis functions are required to calculate its boundaries. Because of a rather strong attraction between B and C in the present case, it is the bcc phase with the B-rich matrix which (out of all other ordered phases) remains stable at the lowest copolymer concentrations and forms the region of three-phase coexistence together with the A-rich and B-rich disordered phases.

The phase behavior (excluding the bcc phases) of the A/B/AC blends, with $\chi_{AB}N_h = 4$, $\chi_{AC}N_h = 3$, and $\chi_{BC}N_h = -1$, is summarized in Figure 9, which shows the $\phi_{Ah} = \phi_{Bh}$ cut through the Gibbs triangles for different values of α. To facilitate the comparison, we have also included in Figure 9 the lamellar boundary for the A/B/AB blend with the same value of $\chi_{AB}N_h = 4$. We see that for a certain range of α, the hexagonal channel of an A/B/AC blend is stable at lower copolymer concentrations than the lamellar phase of the corresponding A/B/AB blend. This decrease in ϕ_c is rather small, and in fact, it changes to the opposite effect when $\alpha < 0.27$.

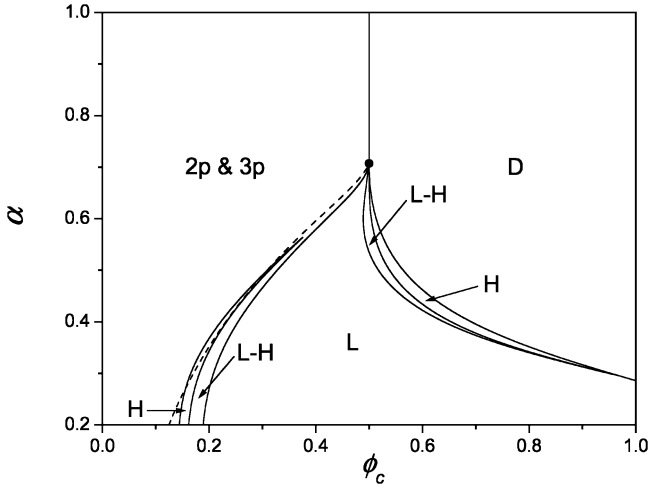

Figure 9. α vs ϕ_c diagram for the compositionally symmetric A/B/AC blends with $\chi_{AB}N_h = 4$, $\chi_{AC}N_h = 3$, and $\chi_{BC}N_h = -1$. Since eq 43 is satisfied, the Lifshitz point (full circle) is identical to that in the reference A/B/AB system (cf. Figure 2). The dashed line shows the lamellar boundary in the same A/B/AB system. Interestingly we observe two different hexagonal phases in this compositionally symmetric system, one of which is the highly swollen phase with the B-rich matrix. Regions of coexistence of the lamellar ("L") and hexagonal ("H") phases are indicated by "L−H". The two-phase and three-phase coexistence regions which involve one or more homogeneous phase are combined for simplicity in one region—marked "2p and 3p".

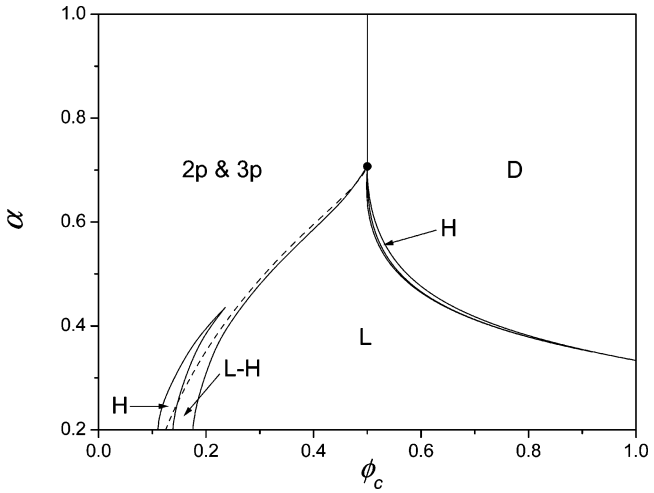

Figure 10. α vs ϕ_c diagram for the compositionally symmetric A/B/AC blends with $\chi_{AB}N_h = 4$, $\chi_{AC}N_h = 3.5$, and $\chi_{BC}N_h = -0.5$. Since the BC attraction is not very strong, it takes fairly long copolymer chains for the hexagonal channel to appear. However it extends to lower copolymer concentrations than the channel in Figure 9 (see also the phase nomenclature in Figure 9).

Figure 10 shows a similar diagram but for $\chi_{AC}N_h = 3.5$ and $\chi_{BC}N_h = -0.5$. The attraction between B and C is not very strong in this case; hence it takes longer copolymer chains for the hexagonal channel to appear. However, once there, this channel extends to lower copolymer concentrations than for the blends with $\chi_{BC}N_h = -1$. Since we associate the hexagonal phase inside the channel with a polymeric microemulsion, we conclude that very strong attractions between B and C are actually not favorable for the formation of such microemulsions.

We observed a qualitatively different phase behavior for the highly segregated blends with $\chi_{AB}N_h = 10$. The corresponding, α vs ϕ_c, phase diagram is shown in Figure 11 for $\chi_{AC}N_h = 7.5$ and $\chi_{BC}N_h = -2.5$. The channel of the hexagonal phase at low concentrations ϕ_c is absent in this case, even far below the Lifshitz point (we have checked this for all $\alpha \geq 0.5$). The absence of the hexagonal channel is also illustrated in Figure 12 which shows the Gibbs triangle for $\alpha = 1$. We see that the B-rich hexagonal phase has a principally different shape than for the blends studied above and, in fact, does not extend to low copolymer concentrations near the $\phi_{Ah} = \phi_{Bh}$ isopleth. Thus, even if this hexagonal phase were observed at $\phi_{Ah} = \phi_{Bh}$ for some $\alpha < 0.5$, it would still have a high copolymer content of about 30−40% and therefore would not be such a good candidate for the formation of microemulsions. We also see from Figures 11 and 12 that the bottom boundary of the lamellar phase recedes to much higher copolymer concentrations than in the respective A/B/AB blends. In general, the lamellar phase covers a fairly short section of the $\phi_{Ah} = \phi_{Bh}$ isopleth, which is

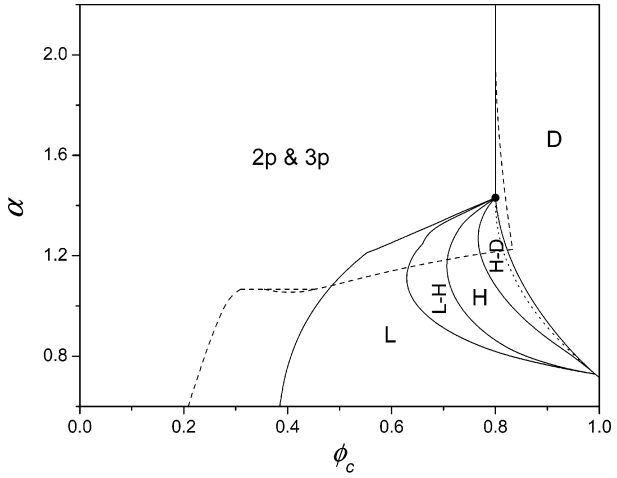

Figure 11. α vs ϕ_c diagram for the compositionally symmetric A/B/AC blends with $\chi_{AB}N_h = 10$, $\chi_{AC}N_h = 7.5$, and $\chi_{BC}N_h = -2.5$. The dashed line follows the contours of the lamellar phase ("L") in the reference A/B/AB system (cf. Figure 5). The region of coexistence of three homogeneous phases is missing from this diagram, so that the boundaries of the ordered structures go through the Lifshitz point (full circle). The origins of the two singularities, observed in these boundaries, are explained in the main text. The dotted section of the spinodal line is included inside the two-phase region ("H−D") which separates the hexagonal phase with the A-rich matrix ("H") from the disordered phase ("D"). Note the absence of the hexagonal phase with the B-rich matrix at low copolymer concentrations.

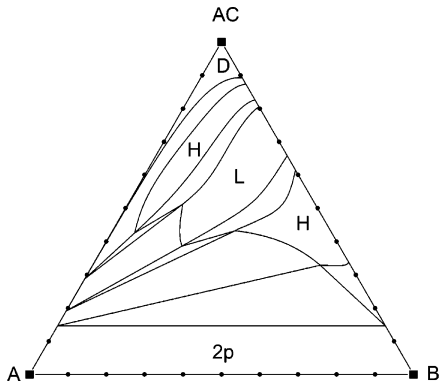

Figure 12. Gibbs triangle for the A/B/AC blend with the same interaction parameters as in Figure 11 and $\alpha = 1$. This diagram is highly asymmetric due to the strong attraction between B and C. The hexagonal phase with the B-rich matrix extends to low copolymer concentrations near the $\phi_{Ah} = 0$ side of the Gibbs triangle, in contrast to Figures 6 and 8 where it occurs in the vicinity of the $\phi_{Ah} = \phi_{Bh}$ isopleth. ("L" is lamellar, "H" is hexagonal, "D" is disordered, and "2p" is liquid−liquid coexistence.)

a result of very strong attractions between B and C. Our initial incentive for choosing a large absolute value of $\chi_{BC}N_h$ was to stabilize at low copolymer concentrations the channel of the B-rich hexagonal phase. However, the side effect of stabilizing the hexagonal phase (with the A-rich matrix) at high copolymer concentrations turned out to be stronger than the desired effect. This latter hexagonal phase covers a relatively large section of the $\phi_{Ah} = \phi_{Bh}$ isopleth and extends all the way up to the $\phi_{Ah} = 0$ side of the Gibbs triangle. For $\chi_{AB}N_h = 10$, we see a strong first-order transition between the hexagonal and disordered phases, accompanied by a wide region of the two-phase coexistence (Figure 11)—whereas in the case of $\chi_{AB}N_h = 4$, it is a very weak first-order transition such that the lines of the two coexisting phases cannot be distinguished from the spinodal line (see Figures 9 and 10).

The two singularities seen in the lamellar boundaries in Figure 11, are the terminal points of the lines separating the regions of two-phase and three-phase coexistence. We did not calculate these lines, since they do not provide additional information on the ordered structures and would require the construction of the full Gibbs triangle for each value of α. To explain the origin of these singularities, we note that the area occupied by the lamellar phase in Figure 11 shrinks when α approaches its value at the Lifshitz point. In Figure 12, this shrinkage is followed by a shift of the two singular points in the lamellar phase boundary—which are also the corners of the corresponding three-phase triangles—to the B-rich part of the Gibbs triangle. The singularities in Figure 11 are given by the values of α when these points touch the $\phi_{Ah} = \phi_{Bh}$ isopleth. At larger values of α, the isopleth is crossed by the section of the lamellar phase boundary which corresponds to the first-order transition to the A-rich homogeneous phase and not, as in Figure 12, to either of the two hexagonal phases. Hence, a sharp change of direction is observed in the boundaries in Figure 11.

Finally, we note that the three-liquid-phase coexistence region is missing from the diagram in Figure 11 and therefore the regions of stability of the ordered phases proceed all the way up to the Lifshitz point. Thus, in the vicinity of the Lifshitz point, the AC diblock copolymers are more effective compatibilizers than their AB counterparts; whereas we observe the opposite effect for smaller values of α. Note that this is a purely thermodynamic picture which takes into account only the stabilizing properties of different copolymers at the interface, but disregards their kinetic abilities to reach this interface.

4. Conclusions and Discussion

We have studied the phase behavior of balanced A/B/AC polymer blends, where C is attracted to B, and compared it with the phase behavior of the reference A/B/AB blends. In the special case of compositionally symmetric diblocks and equal molecular weights of A and B, we can give a quantitative definition of a balanced surfactant, eq 43, which ensures equal A-philic and B-philic tendencies of the AC copolymer chains. For a balanced diblock copolymer, the liquid phase diagrams of the A/B/AC blends are fully symmetric. However, when the ordered structures such as lamellar, hexagonal or bcc, are also taken into account, the attraction between B and C leads to highly asymmetric phase diagrams.

Our main objective was to find a diblock copolymer which would facilitate the mixing of a strongly segregated blend of A and B, while adding the smallest possible amount of it. For this purpose, we have mainly worked with two values of the homopolymer incompatibility parameter, $\chi_{AB}N_h = 4$ and $\chi_{AB}N_h = 10$, both corresponding to a clearly immiscible pair of A and B. We have observed a very different phase behavior in these two cases, both for A/B/AB and A/B/AC blends. The general tendency observed for all blends is that longer copolymer chains are required to improve the compatibilization effect.

In the phase diagrams of the A/B/AC blends with $\chi_{AB}N_h = 4$, we have discovered a narrow channel of the hexagonal phase with the B-rich matrix, crossing the line of symmetric blend compositions. This channel is observed at copolymer concentrations ϕ_c which are only slightly lower than the minimal copolymer content in the reference A/B/AB lamellar phase. However, the free energy of the hexagonal phase inside the channel is lower than the free energy of the reference A/B/AB lamellar phase, if both are calculated for the same blend compositions. Hence we expect that, in experimental applications, the A/B/AC blends will be more stable with respect to macrophase separation than their A/B/AB counterparts, thus creating a possibility for the formation of bicontinuous structures with a small copolymer content.

When considering the A/B/AC blends with $\chi_{AB}N_h = 10$, we have chosen a rather large value of the interaction parameter between species B and C, $\chi_{BC}N_h = -2.5$. Such a large absolute value of χ_{BC} is necessary in this case to bring about significant changes in the corresponding A/B/AB diagrams, and in particular, to stabilize the channel of the hexagonal phase observed for $\chi_{AB}N_h = 4$. However, we find that the hexagonal phase is not stable for symmetric blend compositions, and in addition, the lamellar phase recedes to much higher copolymer concentrations than in the A/B/AB blends. Here, the only advantage of the BC attractions is the presence of ordered structures in the blends where the copolymer chains are shorter than the homopolymers; in the A/B/AB blends such structures are suppressed by the large regions of three-phase coexistence. Overall, however, none of the ordered structures in the A/B/AC blends of symmetric composition are observed for copolymer concentrations smaller than approximately 40%, which is not indicative of a very good compatibilizer. In contrast, in the A/B/AB blends (with diblocks longer than the homopolymers) the lamellar phase creates a striking intrusion into the region of small copolymer concentrations. This vast expansion of the lamellar phase is, in fact, associated with the first-order transition between two distinctly different lamellar phases, which did not appear in the case of $\chi_{AB}N_h = 4$. Thus, according to our thermodynamic theory, for small α the AB diblock copolymers are much more efficient compatibilizers for a pair of highly immiscible homopolymers A and B, than the AC diblocks. This seems to contradict the experimental findings in ref 15, unless the absolute value of χ_{BC} in this experiment is so small that the phase behavior of the symmetric system is essentially reproduced. On the other hand, the experimental results of ref 11—which show that AC diblock copolymers can be better compatibilizers than AB diblocks—in fact have been obtained for copolymer chains that are shorter than the homopolymers and therefore support our results.

Let us now discuss in more detail the possible effects of thermal fluctuations on the formation of bicontinuous structures in ternary polymer blends. In the majority of experimental studies where polymeric microemulsions have been observed,[12−14] the compositions of the examined A/B/AB blends were close to their mean-field Lifshitz compositions. It has also been argued that, although the Lifshitz points themselves can be very accurately located by the mean-field theory, the order−disorder transition temperature near these points is suppressed dramati-

cally by thermal fluctuations.[12,31] Therefore, in polymer blends with nearly Lifshitz compositions, a highly fluctuating disordered phase can exist at very low temperatures, and as confirmed experimentally,[12] this phase has a fully bicontinuous morphology. We may also argue that, as the Lifshitz point is approached along the order−disorder transition line, the spatial period D of the lamellar phase at the transition should become very large. The A/B interfaces in such a lamellar phase can bend easily without perturbing each other, which could result in the loss of long-range order and in the formation of a bicontinuous microemulsion. However, the Lifshitz points can be accessed experimentally only for moderately segregated A/B/AB polymer blends and, quite conveniently, the Lifshitz compositions for such blends are characterized by low copolymer concentrations. If the incompatibility between A and B is increased, the isotropic Lifshitz points move to higher copolymer concentrations and, eventually, are absorbed by the coexistence region of three different homogeneous phases (cf. Figures 2 and 5). On the other hand, the lamellar spacing D can also become large away from the Lifshitz point, for instance, if the lamellar phase gets swollen by a large amount of relatively short homopolymer. The latter scenario should apply also for strongly segregated blends, as verified by the experiment in ref 15, provided of course that a lamellar phase (or a hexagonal phase with interfaces of very low curvature) can be stabilized at low copolymer concentrations. At this point the SCFT can be used to predict those blend parameters which would favor the formation of ordered structures with minimal copolymer content. However, to check the actual stability of a microemulsion phase, it is necessary to calculate its free energy taking into account fluctuations in the interface configurations and spacings. The polymeric microemulsion will only be stable if the resulting free energy is sufficiently lower, on the scale of thermal fluctuations, than the free energy of the macrophase separated blend.

To summarize our results, we find that largely swollen lamellar and/or hexagonal phases appear in A/B/AC blends (where C may equal B) if (i) the copolymers are long relative to the homopolymers, (ii) the balance condition (43) is satisfied, and (iii) the absolute value of χ_{BC} is not too large. We conclude that blends with the above characteristics are the best candidates for the formation of polymeric microemulsions with low copolymer content. In the case of moderate segregation between A and B, $\chi_{AB}N_h \approx 4$, the A/B/AC blends are expected to mix slightly better than their A/B/AB counterparts, and we anticipate that a bicontinuous microemulsion may form at $\phi_c \lesssim 20\%$ (Figure 10). At larger segregations, $\chi_{AB}N_h \approx 10$, the phase behavior of A/B/AB and A/B/AC blends should be very similar for relatively small absolute values of $\chi_{BC}N_h$. In this case we expect that a bicontinuous microemulsion may form at $\phi_c \lesssim 40\%$ (Figure 5). Indeed, we find that in this region of copolymer concentrations, the free energy of the lamellar phase is almost independent of its spacing D, or copolymer content ϕ_c, so that a very large number of different lamellar phases can coexist at the same time with no free energy cost. This is in full agreement with the previous SCFT calculations by Kodama et al.[39] who, in the A/B/AB polymer blend with $\chi_{AB}N_h = 8$ and $\alpha = 0.5$, find a metastable microemulsion phase at $\phi_c = 40\%$ as well as a marginally stable lamellar phase at $\phi_c < 40\%$. A definite conclusion of the SCFT is that a polymeric microemulsion with low copolymer content will not form if the absolute value of $\chi_{BC}N_h$ is large. However, in this case, the Lifshitz point is no longer "hidden" in the A/B/AC blends, as opposed to the symmetric A/B/AB blends, and it can therefore be accessed experimentally (Figure 11). Nevertheless, if a microemulsion phase were to form in the vicinity of this Lifshitz point, it would have a very high copolymer content and would combine the properties of all three chemical species, rather than just A and B. Besides, the required large amounts of copolymer would make it costly to produce.

In real experiments, the thermodynamic picture described above will be complicated by the kinetic factors. This will lead to the existence of an optimal degree of polymerization of copolymer chains, which will balance their compatibilizing properties and the ability to reach the interface.[40] There has also been some experimental evidence that the kinetic factors are, in fact, dependent on the side of the interface to which the copolymer is introduced.[41]

Finally, we note that it is only for symmetric blend compositions that either AB or AC may serve as a better compatibilizer, which depends sensitively on the specific blend parameters. Whereas, if we wish to dissolve a small amount of A in the B-rich matrix, then any AC copolymer whose C block is attracted to B, is clearly a more advantageous choice.

A. Basis Sets for the Lamellar, Hexagonal, bcc, and Gyroid Phases

The Fourier harmonics for different symmetry groups can be found in ref 29. For the lamellar, hexagonal, bcc ($Q_{Im\bar{3}m}$), and gyroid ($Q_{Ia\bar{3}d}$) phases they are, in respective order

$$f(x, h) = C(h)\cos 2\pi hx, \quad h \geq 0 \tag{49}$$

$$f(x, y, h, k) = C(h, k)\left(\cos\frac{2\pi(h-k)y}{\sqrt{3}}\cos 2\pi(h+k)x + \cos\frac{2\pi(h+2k)y}{\sqrt{3}}\cos 2\pi hx + \cos\frac{2\pi(k+2h)y}{\sqrt{3}}\cos 2\pi kx\right), \quad h \geq k \geq 0 \tag{50}$$

$$f(x, y, z, h, k, l) = C(h, k, l)(\cos 2\pi hx \cos 2\pi ky \cos 2\pi lz + \cos 2\pi hx \cos 2\pi ly \cos 2\pi kz + \cos 2\pi hy \cos 2\pi kz \cos 2\pi lx + \cos 2\pi hy \cos 2\pi lz \cos 2\pi kx + \cos 2\pi hz \cos 2\pi kx \cos 2\pi ly + \cos 2\pi hz \cos 2\pi lx \cos 2\pi ky), \quad h + k + l = 2n, \quad h \geq k \geq l \geq 0 \tag{51}$$

$$f'(x, y, z, h, k, l) = C'(h, k, l) \times \cos\frac{\pi(h+k+l)}{2}\left\{\cos 2\pi\left(hx + \frac{l}{4}\right)\cos 2\pi\left(ky + \frac{h}{4}\right)\cos 2\pi\left(lz + \frac{k}{4}\right) + \cos 2\pi\left(kx + \frac{h}{4}\right)\cos 2\pi\left(ly + \frac{k}{4}\right)\cos 2\pi\left(hz + \frac{l}{4}\right) + \cos 2\pi\left(lx + \frac{k}{4}\right)\cos 2\pi\left(hy + \frac{l}{4}\right)\cos 2\pi\left(kz + \frac{h}{4}\right) + \cos\frac{\pi(h+k+l)}{2}\left[\cos 2\pi\left(hx + \frac{k}{4}\right)\cos 2\pi\left(ly + \frac{h}{4}\right)\cos 2\pi\left(kz + \frac{l}{4}\right) + \cos 2\pi\left(kx + \frac{l}{4}\right)\cos 2\pi\left(hy + \frac{k}{4}\right)\cos 2\pi\left(lz + \frac{h}{4}\right) + \cos 2\pi\left(lx + \frac{h}{4}\right)\cos 2\pi\left(ky + \frac{l}{4}\right)\cos 2\pi\left(hz + \frac{k}{4}\right)\right]\right\}, \quad h + k + l = 2n, \quad h \geq k \geq l \geq 0 \tag{52}$$

where h, k, l, and n are all integers and the coefficients C and C' are chosen to satisfy the orthonormalization condition in eq 20 of the main text.

B. Random Phase Approximation. We start with the structure factor matrix $\hat{G}$ of an ideal ternary blend which takes

the form

$$\hat{G}(\boldsymbol{q}) = \begin{vmatrix} G^{c}_{AA} & G_{AC} & 0 & 0 \\ G_{AC} & G_{CC} & 0 & 0 \\ 0 & 0 & G^{h}_{AA} & 0 \\ 0 & 0 & 0 & G_{BB} \end{vmatrix} \tag{53}$$

where the matrix indices $i = 1, 2$ stand for the copolymer blocks A/C, and $i = 3, 4$ for the homopolymers A/B, respectively. The individual contributions in eq 53 are

$$N^{-1}G^{h}_{AA} = \phi_{Ah}\alpha_A g(1,\alpha_A Q) \tag{54}$$

$$N^{-1}G^{c}_{AA} = \phi_c g(f, Q) \tag{55}$$

$$N^{-1}G_{AC} = \frac{\phi_c}{2}[g(1, Q) - g(f, Q) - g(1 - f, Q)] \tag{56}$$

$$N^{-1}G^{h}_{BB} = \phi_{Bh}\alpha_B g(1,\alpha_B Q) \tag{57}$$

$$N^{-1}G_{CC} = \phi_c g(1 - f, Q) \tag{58}$$

where $Q = q^2 R_G^2$, R_G being the copolymer radius of gyration, and $g(f, x)$ is the Debye function

$$g(f, x) = \frac{2}{x^2}[\exp(-fx) + fx - 1] \tag{59}$$

The definitions of the blend parameters featured in eqs 54−58, are given in the main text. The structure factor of an interacting polymer blend is given by

$$\hat{S}(\boldsymbol{q}) = (\hat{G}^{-1}(\boldsymbol{q}) + \hat{c}(\boldsymbol{q}))^{-1} \tag{60}$$

where $\hat{c}$ is the interaction matrix

$$\hat{c} = \begin{vmatrix} c_0 & \chi_{AC} + c_0 & c_0 & \chi_{AB} + c_0 \\ \chi_{AC} + c_0 & c_0 & \chi_{AC} + c_0 & \chi_{BC} + c_0 \\ c_0 & \chi_{AC} + c_0 & c_0 & \chi_{AB} + c_0 \\ \chi_{AB} + c_0 & \chi_{BC} + c_0 & \chi_{AB} + c_0 & c_0 \end{vmatrix} \tag{61}$$

The additive constant

$$c_0 = \frac{1}{1 - \Phi} \tag{62}$$

where Φ is the total polymer fraction, is included in order to fulfill the incompressibility constraint. This is done by taking the $\Phi \rightarrow 1$ limit in the final expression for $\hat{S}(\boldsymbol{q})$ which results from combining eqs 53, 60, and 61. After some algebra we find

$$\hat{S} = \frac{\hat{\sigma}}{s_1 s_2 + s_2 s_3 + s_1 s_3} \tag{63}$$

where

$$\hat{\sigma} = \begin{vmatrix} \sigma_{11} & \sigma_{12} & \sigma_{13} & \sigma_{14} \\ \sigma_{12} & [s_1 + s_2] & -[s_1 + \sigma_{12}] & -s_2 \\ \sigma_{13} & -[s_1 + \sigma_{12}] & \sigma_{33} & \sigma_{34} \\ \sigma_{14} & -s_2 & \sigma_{34} & [s_2 + s_3] \end{vmatrix} \tag{64}$$

The individual contributions in eq 64 are

$$s_1 = \frac{1}{G_{BB}} - \frac{G_{AC}}{G_{AA}G_{CC} - G_{AC}^2} + K_1 \tag{65}$$

$$s_2 = \frac{G_{AC} + G_{CC}}{G_{AA}G_{CC} - G_{AC}^2} + K_2 \tag{66}$$

$$s_3 = \frac{G_{AC} + G_{AA}}{G_{AA}G_{CC} - G_{AC}^2} + K_3 \tag{67}$$

where $G_{AA} \equiv G^{h}_{AA} + G^{c}_{AA}$, and

$$\sigma_{11} = \eta^{-1}(\beta\delta + \beta\gamma + \gamma\delta) \tag{68}$$

$$\sigma_{12} = \eta^{-1}(-\gamma\delta - \epsilon\delta - \epsilon\gamma + K_2\delta) \tag{69}$$

$$\sigma_{13} = \eta^{-1}(-\beta\delta + \epsilon\delta - K_2\beta - K_2\delta) \tag{70}$$

$$\sigma_{14} = -\sigma_{11} - \sigma_{12} - \sigma_{13} \tag{71}$$

$$\sigma_{33} = s_1 + s_3 - \sigma_{11} - 2\sigma_{13} \tag{72}$$

$$\sigma_{34} = \sigma_{11} + \sigma_{12} + \sigma_{13} - s_3 \tag{73}$$

where

$$\beta = \frac{G^{c}_{AA}}{G^{c}_{AA}G_{CC} - G_{AC}^2} + K_3 \tag{74}$$

$$\gamma = \frac{1}{G^{h}_{AA}} + K_2 \tag{75}$$

$$\delta = \frac{1}{G_{BB}} + K_1 \tag{76}$$

$$\epsilon = -\frac{G_{AC}}{G^{c}_{AA}G_{CC} - G_{AC}^2} \tag{77}$$

$$\eta = \frac{G_{CC}}{G^{c}_{AA}G_{CC} - G_{AC}^2} + \frac{1}{G^{h}_{AA}} \tag{78}$$

The parameters K_1, K_2, and K_3 are defined in eq 32 of the main text. The resulting scattering profile from an A/B/AC polymer blend is given by

$$I(\boldsymbol{q}) = \vec{B}^{T}\hat{S}(\boldsymbol{q})\vec{B} \tag{79}$$

where $\vec{B}$ is the column vector describing the contrast. Equations 63, 64, and 79 can be used to fit experimental scattering curves with four independent fitting parameters: K_1N, K_2N, K_3N, and R_G^2.

Acknowledgment. We would like to thank Hitoshi Endo, Dietmar Schwahn, Lutz Willner, and Dieter Richter (Forschungszentrum Jülich) for many stimulating and fruitful discussions, involving their experimental work on polymeric microemulsions. We are also indebted to Daniel Duque (Institut de Ciencia de Materials de Barcelona) for his helpful advice on how to improve our numerical code.

References and Notes

(1) Creton, C.; Kramer, E. J.; Brown, H. R.; Hui, C. Y. *Adv. Polym. Sci.* **2001**, *156*, 53.
(2) Koning, C.; Van Duin, M.; Pagnoulle, C.; Jerome, R. *Prog. Polym. Sci.* **1998**, *23*, 707.
(3) Ruzette, A. V.; Leibler, L. *Nat. Mater.* **2005**, *4*, 19.

(4) Kahlweit, M.; Strey, R. *Angew. Chem., Int. Ed. Engl.* **1985**, *24*, 654.
(5) Gompper, G.; Schick, M. In *Phase Transitions and Critical Phenomena*; Domb, C., Lebowitz, J., Eds.; Academic Press: London, 1994; Vol. 16, p 1.
(6) Bates, F. S.; Fredrickson, G. H. *Annu. Rev. Phys. Chem.* **1990**, *41*, 525.
(7) Kinning, D. J.; Wilney, K. I.; Thomas, E. L. *Macromolecules* **1988**, *21*, 3502.
(8) Koizumi, S.; Hasegawa, H.; Hashimoto, T. *Macromolecules* **1994**, *27*, 6532.
(9) Matsen, M. W. *Macromolecules* **1995**, *28*, 5765.
(10) Matsen, M. W. *Phys. Rev. Lett.* **1995**, *74*, 4225.
(11) Chun, S. B.; Han, C. D. *Macromolecules* **1999**, *32*, 4030.
(12) Bates, F. S.; Maurer, W. W.; Lipic, P. M.; Hillmyer, M. A.; Almdal, K.; Mortensen, K.; Fredrickson, G. H.; Lodge, T. P. *Phys. Rev. Lett.* **1997**, *79*, 849.
(13) Schwahn, D.; Mortensen, K.; Frielinghaus, H.; Almdal, K.; Kielhorn, L. *J. Chem. Phys.* **2000**, *112*, 5454.
(14) Morkved, T. L.; Stepanek, P.; Krishnan, K.; Bates, F. S.; Lodge, T. P. *J. Chem. Phys.* **2001**, *114*, 7247.
(15) Lee, J. H.; Balsara, N. P.; Krishnamoorti, R.; Jeon, H. S.; Hammouda, B. *Macromolecules* **2001**, *34*, 6557.
(16) Lee, J. H.; Ruegg, M. L.; Balsara, N. P.; Zhu, Y.; Gido, S. P.; Krishnamoorti, R.; Kim, M. *Macromolecules* **2003**, *36*, 6537.
(17) Reynolds, B. J.; Ruegg, M. L.; Balsara, N. P.; Radke, C. J.; Shaffer, T. D.; Lin, M. Y.; Shull, K. R.; Lohse, D. J. *Macromolecules* **2004**, *37*, 7401.
(18) Fayt, R.; Jerome, R.; Teyssie, P. *J. Polym. Sci., Part B: Polym. Phys.* **1989**, *27*, 775.
(19) Adedeji, A.; Hudson, S. D.; Jamieson, A. M. *Polymer* **1997**, *38*, 737.
(20) Müller, M.; Schmid, F. *Adv. Polym. Sci.* **2005**, *185*, 1.
(21) Matsen, M. W. In *Soft Matter*; Gompper, G.; Schick, M., Eds.; Wiley-VCH: Weinheim, Germany, 2005; Vol. 1, p 87.
(22) de Gennes, P. G.; Taupin, C. *J. Phys. Chem.* **1982**, *86*, 2294.
(23) Morse, D. C. *Curr. Opin. Colloid Interface Sci.* **1997**, *2*, 365.
(24) Gompper, G.; Kroll, D. M. *Phys. Rev. Lett.* **1998**, *81*, 2284.
(25) Reynolds, B. J.; Ruegg, M. L.; Mates, T. E.; Radke, C. J.; Balsara, N. P. *Macromolecules* **2005**, *38*, 3872.
(26) Matsen, M. W.; Schick, M. *Phys. Rev. Lett.* **1994**, *72*, 2660.
(27) Janert, P. K.; Schick, M. *Macromolecules* **1997**, *30*, 137.
(28) Grosberg, A. Yu.; Khokhlov, A. R. *Statistical Physics of Macromolecules*; American Institute of Physics: New York, 1994.
(29) *International Tables for X-ray Crystallography*; Henry, N. F. M., Lonsdale, K., Eds.; Kynoch: Birmingham, U.K., 1969; Vol. 1.
(30) Broseta, D.; Fredrickson, G. H. *J. Chem. Phys.* **1990**, *93*, 2927.
(31) Fredrickson, G. H.; Bates, F. S. *J. Polym. Sci., Part B: Polym. Phys.* **1997**, *35*, 2775.
(32) Scott, R. L. *J. Chem. Phys.* **1949**, *17*, 279.
(33) Olsson, U.; Würz, U.; Strey, R. *J. Phys. Chem.* **1993**, *97*, 4535.
(34) Holyst, R.; Schick, M. *J. Chem. Phys.* **1992**, *96*, 7728.
(35) Janert, P. K.; Schick, M. *Macromolecules* **1997**, *30*, 3916.
(36) Naughton, J. R.; Matsen, M. W. *Macromolecules* **2002**, *35*, 8926.
(37) de Gennes, P. G. *Scaling Concepts in Polymer Physics*; Cornell University: Ithaca, NY, 1979.
(38) Hornreich, R. M.; Luban, M.; Shtrikman, S. *Phys. Rev. Lett.* **1975**, *35*, 1678.
(39) Kodama, H.; Komura, S.; Tamura, K. *Europhys. Lett.* **2001**, *53*, 46.
(40) Galloway, J. A.; Jeon, H. K.; Bell, J. R.; Macosko, C. W. *Polymer* **2005**, *46*, 183.
(41) Retsos, H.; Anastasiadis, S. H.; Pispas, S.; Mays, J. W.; Hadjichristidis, N. *Macromolecules* **2004**, *37*, 524.

MA060364X